# A Feasibility Study of Micromachined Ultrasonic Transducers Functionalized for Ethanol Detection

by

Yaning Cui

A thesis
presented to the University of Waterloo
in fulfillment of the
thesis requirement for the degree of
Master of Applied Science
in
Systems Design Engineering (Nanotechnology)

Waterloo, Ontario, Canada, 2017

# AUTHOR'S DECLARATION

I hereby declare that I am the sole author of this thesis. This is a true copy of the thesis, including any required final revisions, as accepted by my examiners.

I understand that my thesis may be made electronically available to the public.

# Abstract

The chemical sensing system plays an important role in medical and environmental monitoring. Gases exhaled by humans include nitrogen, oxygen, water vapor, carbon dioxide and volatile organic compounds (VOCs). The VOCs are important and provide valuable information for non- invasive diagnosis. For instance, ethanol detection is beneficial for checking blood alcohol. In time blood alcohol level checking before checking can prevent a person from unsafe driving.

Due to the extremely low concentration of the target gases, a gas sensor with high sensitivity, selectivity and low detection limit is required. There is a high demand for low cost, fast, accurate and easy-to-use self-check diagnosis devices. With low cost and high portability, micro-electromechanical systems (MEMS) sensors have been extensively studied for chemical sensing, which provide a cheap self-diagnosis solution.

Capacitive Micromachined Ultrasonic Transducers (CMUTs) and Piezoelectric Micromachined Ultrasonic Transducer (PMUTs), which both work based on the mass-loading effect, are considered as the promising types of MEMS sensors for gas sensing. Since they are fabricated in a batch manner with the similar process of silicon-based integrated circuits, CMUTs and PMUTs are able to provide massive parallelism, easy integration with microelectronic circuits, and a higher quality factor.

In this research, studied the feasibility of using PMUTs and CMUTs fabricated by our lab for ethanol detection through simulation and experiments. Models for are built via COMSOL for PMUT and CMUT respectively. The simulation results of a single sensing element demonstrated that both CMUTs and PMUTs show great potential for gas sensors. The chemical experiments through frequency response measurement exhibit that both the PMUTs and CMUTs are effective for ethanol detection based on the mass-loading effect. When the gas analyte is attached to the sensing layer, a higher resonance frequency of the transducer induces a higher frequency shift, which means the higher resonance frequency of transducer, the higher sensitivity of a gas sensor is and the lower concentration of ethanol can be detected. Additionally, a CMUT array is also applied to ethanol detection. It provides a good preliminary study of the CMUTs functionalized with more sensing materials for chemical detection in future.

# Acknowledgements

The work conducted in the thesis would not have been possible without the suggestions, guidance, and helps from many people.

First and foremost, I would like to show my deepest gratitude to my supervisor, Prof. Yeow, for giving me the opportunity to be involved in his research and to work on the interesting project. Thank you for supporting finance and all equipment/materials. Without these resources that support my project, I would not have been able to finish this feasibility study. His vigorous academic observation enlightens me not only in this thesis but also in my future study. I would also like to thank the other members of my committee- Prof. Eihab Abdel-Rahman and Prof. William W. Melek for serving as my second readers. In addition, I sincerely thank Prof. Eihab Abdel-Rahman for allowing me to use the vibrometer in his lab.

Second, to my colleagues, I would like to acknowledge that you are some of the most amazing people that left a deep impression in my life. I am very pleased and honoured working with you guys. I particularly thank Zhenhao Li, whom I closely work with for this project. You gave me many direct and indirect helps to my research. Thanks for always replying to my questions, and being a great teacher. Also thanks to Lawrence Wong, Albert Chen, and Nash Shuai who introduce me to the wonderful world of CMUTs. You taught me how to do researches, analyze problems, and propose solutions. I will never forget the time working with you. All other lab mates: Chen, Joe, Champika, Fred, Mingyu, Siyuan, Yunhan, Yibei, Limin. Thank you all for the help in the past few years and nice meeting you.

Furthermore, I would like to thank my beloved family for all the support and encouragement over the past two years. I tear up every time I think about how wonderful you are and how lucky I am to be your child.

Lastly, and most importantly, I want to thank my boyfriend, Peng, for being on my side all the time to keep me going on. I would not have been able to make it this far without you.

Thank you, everyone!

# Table of Contents

# List of Figures

# List of Tables

# Chapter 1
# Introduction and Outline

## 1.1 Introduction

Driving under the influence of alcohol is a major problem, which results in great numbers of casualties and deaths every year [1]. A survey in 2016 demonstrates that across Canada, police reported 74,800 driving incidents induced by alcohols or drug in 2014, while of those cases, 97% involved alcohol, which occupies a large proportion. Furthermore, these accidents cost billions of dollars every year in the economy [2].

In order to solve this problem, self-check of blood alcohol content (BAC) is important for drivers to secure their driving safety through exhaled ethanol detection. Currently, one aggressive method to avoid drunk driving is ignition interlock systems in vehicles [3]. It detects the driver's breath alcohol concentration before starting the car rather than throughout a journey by using a breath alcohol detector. The current ignition interlock systems in vehicles are only required by court order, which makes people feel guilty. Additionally, they are very bulky and quite expensive. It is hardly to be accepted by the public to prevent a person from driving while intoxicated.

Therefore, a portable and accurate ethanol sensor that is able to monitor the driver's breath alcohol concentration whenever would benefit. One of the effective solutions proposed by pervious study is a wearable epidermal ethanol sensor [4].

A chemical sensor always consists of a sensing material and a transducer. The sensing material decides the chemical analyte. The transducer converts the chemical information to other signals. A good chemical sensor is desired to be both sensitive and selective. This thesis focuses on Micro-electromechanical systems (MEMS) chemical sensors. It investigates a feasibility study of Micromachined Ultrasonic Transducers (MUTs) functionalized with sensing films for ethanol detection.

## 1.2 Outline

The first chapter is an introduction to the thesis. It discusses the motivation for this study. Furthermore, the first chapter outlines what is presented in subsequent sections.

The second chapter demonstrates relevant literature background. In the second chapter, it begins with the volatile organic compounds (VOC) detection, and specifically talking about the ethanol detection. Types sensing materials are introduced as well as MEMS Chemical Sensors. Since the study of ethanol detection is based on MUTs, some knowledge of them is presented. This section includes two different type of transducers: Capacitive Micromachined Ultrasonic Transducers (CMUTs) and Piezoelectric Micromachined Ultrasonic Transducers (PMUTs) with following aspects: the basic structures, fundamentals of operation, applications and fabrication methods.

The third chapter explains the general principle of operation by using CMUTs and PMUTs for ethanol detection. The two main factors of a chemical sensor are illustrated in this part as well.

The fourth chapter particularly presents how the CMUTs and PMUTs work for ethanol detection, which is the core of the thesis. It starts with a description of the current transducers fabricated by our lab for gas sensing with details. The mass-loading effect is analyzed firstly by exploring the relationship of resonance frequency and mass of transducers. In order to illustrate the principle of gas sensing directly, it is considered in Finite Element Method (FEM) model.

Then, in the fifth chapter an experimental test system is designed to evaluate complete ethanol sensors (transducers covered with sensing materials). It includes the depositions of the sensing material and the experimental procedures of ethanol detection. The performance of sensing layer is characterized by observing under scanning electron microscope (SEM). The results from chemical experiment demonstrate a feasibility study of CMUTs and PMUTs for ethanol sensing.

The last chapter summarizes the work and suggests some future directions for further studies.
Literature Background.

# Chapter 2
# Literature Background

## 2.1 Volatile Organic Compound Detection

Gasses exhaled by humans include nitrogen, oxygen, water vapor, carbon dioxide and volatile organic compounds (VOCs). VOCs have been attracting researchers' attention due to its ability to provide valuable information which can be applied to a variety of applications. Acetone detection is widely used for non-invasive diagnosis. A rise of the concentration of acetone presented on a person always indicates a high possibility of suffering from heart failure [5]. Additionally, Formaldehyde and Benzene detection can be applied to indoor air quality monitoring [6]. Ethanol detection is adopted by traffic enforcement, which has saved thousands of lives [7].

VOC detection can also be applied for food safety. Detecting methanol for example, alcohols mainly contains ethanol. Due to the relative lower cost of methanol, some unscrupulous manufacturers might use methanol to take a place of the ethanol. Since the odor of methanol is similar to ethanol, it's difficult for people to distinguish from two compounds. Ingestion of methanol results in blinding or even death, thus an effective detector is required.

As for all efficient sensors, low limited detection, high sensitivity, selectivity are the key requirements for VOCs detection in organic gases. These features depend on both sensing materials and transducers. Therefore, highly sensitive and selective sensing materials and sensors are required.

## 2.2 Sensing Materials

The most important part of a gas sensor is the sensing materials because the sensing target is interacted and decided by the selectivity of the sensing material. In typical gas sensing systems, the transducer is coated with specific sensing material, and then the gas molecule with a concentration interacts with the sensing material through "sorption" (adsorption or absorption). Adsorption is defined as a gas sticking to the surface of the sensing material, while absorption is a gas diffusing into the interstitial spaces of sensing material layer [7]. For example, the Polyaniline (PANI) interacts with ethanol through adsorption and absorption, as shown in Figure 2-1.

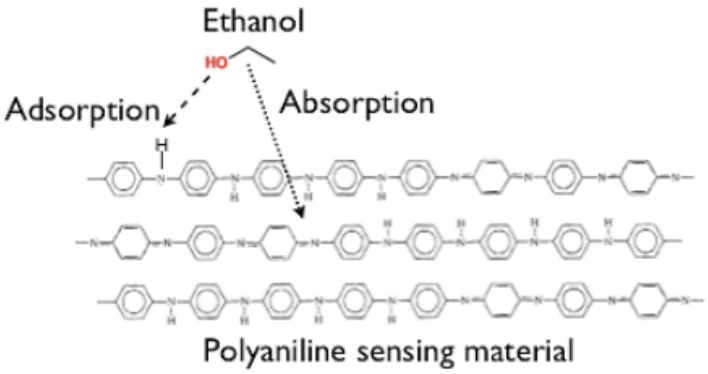


Figure 2-1 Adsorption and absorption of PANI for ethanol detection [7]

A large number of materials can be used as sensing materials for gas sensing. Although different sensing materials own different sensing mechanisms, their unified goal is to help the transducers to convert gas information to other signals. Changing the sensing material on a senor enable it to detect different chemical analytes. The commonly used gas sensing materials are summarized in general in Table 2-1 [8].

Table 2-1 Features of different sensing materials

| Materials | Advantages | Disadvantages |
|---|---|---|
| Metal oxide | ● Low cost<br>● Good reproducibility | ● High operation temperature<br>● High operation voltage<br>● Less sensitive to organic gas |
| Carbon Nanotubes | ● Fast response time<br>● Small and low power consumption | ● Low gas selectivity<br>● Low stability and reproducibility |
| Polymers | ● Low cost<br>● Non-toxic<br>● Easy synthesize | ● Relatively low selectivity (could be improved) |

As it can be learned from the table, they all have positives and negatives. For instance, the metal oxide is the most common sensing material for most inorganic gases, which provides gas sensors with some benefits such as low cost and high sensitivity. The operation principle of the sensors

functionalized with metal oxide for gas sensing is based on the redox reactions between a target gas and the oxide layer [8][9]. The redox reactions depend on some features such as structure of oxide layer and temperature, which decides the sensitivity of metal oxides as sensing materials. For most metal oxide materials the reactions are occurred under high working temperatures, which increases costs and complicates configurations [11]. The polymeric sensing materials exhibit significantly great sensitivity to organic gases, which are ideal materials for VOCs detection. Additionally, their cost is relatively low, because they are easy to be synthesized and can sense target at room temperature.

## 2.3 MEMS Chemical Sensors

The chemical sensor systems have been developed over the years with a wide variety of applications in environmental and safety monitoring, which is necessary to the general public and businesses. A chemical sensor with good performances is considered that should feature a high sensitivity and selectivity. Initially, chemical sensors with good performance are used for gas leak detection in industries. The conventional device, such as ionization gas sensor, is usually bulky, heavy, much high power consumption, and breakdown voltage, which is inefficient and risky in operation [12]. Moreover, because of the emerging applications in the following areas: environmental studies (e.g., greenhouse gas monitoring) [13]; smart home (e.g., detection of benzene) [14]; medical monitoring (e.g., VOCs detection) [15], additional characteristics including low cost as well as portability are required. Therefore, the micro-electromechanical systems (MEMS) technology with the advancement of miniaturized and fully integrated chemical sensors has been received considerable interests to address the rising demands of both industry and academia.

### 2.3.1 Non-resonant Chemical Sensors

MEMS sensors for chemical detection can be classified into two categories that are non-resonant chemical sensors and resonant chemical sensors. The metal oxide semiconductors have been applied as the most common sensing material for non-resonant chemical sensors since 1962. At temperature elevates, the properties of the metal oxide material become sensitive to a particular target gas [16]. As a result of the absorption or desorption of chemical substance on the surface of metal oxide layer, the charge carrier concentration of material has been changed, which alters the conductivity of the material [17]. The metal-oxide gas sensor is highly desirable because of its relatively low cost and

good performance. However, there are some limitations in chemical detection. Firstly, the operational temperature and voltage are relatively high, compared with other devices. Secondly, the choice of metal oxide materials is limited to detectable gas. They could be obviously sensitive to inorganic gas and a few kinds of VOCs such as alcohol, but some of VOCs that might affect health when their concentration is beyond a primary threshold are difficult to be detected by metal oxide [8]. Besides, the metal oxide semiconductors are difficult to integrate with CMOS process.

Therefore, more flexible chemical sensors have been developed to improve the selection of chemicals by using different gas selecting materials, such as organic materials and nanoparticles. For example, polymer-based gas sensors have been studied for many decades. They are frequently applied in detecting inorganic gas like $CO_2$ as well as a wide range of VOCs, such as alcohols, aromatic compounds [8]. Compared with the metal-oxide sensors, they can be expected to operate at room temperature. When the polymer material is exposed to a gas target in air, the physical properties of the polymer such as its mass, resistivity, conductivity or more will alter as the change of gas absorption. It can be measured directly or transformed to a characterization of transducer properties, for instance, the frequency shift of a MEMS resonator.

### 2.3.2 Resonant Chemical Sensors

The resonant transducers functionalized with sensing layers for chemical detection have drawn more attentions in recent years. The principle of operation is the mass-loading effect, which will be demonstrated in detail later. These resonant transducers offer multiple advantages of miniaturization and a wider selection of sensing materials, compared with non-resonant chemical sensors. There are four classic types of sensors that can be used for gas sensor design: 1) Bulk acoustic wave (BAW) resonators; 2) Surface acoustic wave (SAW) resonators; 3) MEMS cantilever beams; 4) Micromachined ultrasonic transducers (MUTs).

Initially, Chemical sensors based on resonators come into two major designs, BWA and SAW. BWA resonator was firstly investigated for chemical detection. Quartz Crystal Microbalance (QCM) is a typical BAW mass sensor [18]. It consists of a thin layer of quartz crystal cut in particular angle with two electrode plates clamping on two sides. When the oscillated electric field between two electrode plates is applied, the quartz crystal can generate acoustics wave. For chemical detection, a thin quartz crystal is covered with a gas sensing film. The absorption of a chemical analyte on crystal

surface serves to result in the resonant frequency shift of transducers, which is proportional to the mass change. However, the mass sensitivity depends on the fundamental frequency of the resonator. It is desirable to cut a thinner quartz crystal to get a higher fundamental frequency of resonators, but there is a difficulty in fabrication. Thus the thickness of the cut crystal will limit the application of BAW resonators in gas detection.

SAW resonators development began in the 1960s [19]. The SAW sensors are composed of two electrode pairs separated by a certain distance from each other on a piezoelectric substrate [20]. The acoustic wave is generated by one electrode pair and propagate along the delay line where the region between the electrodes until being received by another one. A gas sensing film can be deposited on the delay line varying the velocity and resonant frequency of the acoustic wave to detect the loaded mass on the sensing film. Both BAW and SAW sensors have the advantages of being rather relatively sensitive, low cost and miniaturized. The remaining limitation for them is low selectivity because of the availability of coating sensing films.

MEMS cantilever beams can be applied for chemical detection as well. The bending of the cantilever can be produced by different ways such as electrostatic or magnetic actuation force, which can be detected by piezoresistive layers [19]. This fundamental resonant structure can be achieved by a relatively simple fabrication process, which can also be integrated with electronics. Furthermore, It can be fabricated as an array to enable to deposit different sensing films on a transducer. However, the detection of micro-deformation of the beam limits the performance, because the weak signal generated is hard to capture from the parasitic noise, which limits the sensor resolution [16]. It is also noticed that the beam structure might be very fragile which can be easily damaged by miss operation, such as when the beam is pull-in.

Micromachined ultrasonic transducers offer an alternative to traditional crystal based transducers, which are also strong candidates for resonant chemical sensors. There are two conventional transducers, Capacitive Micromachined Ultrasonic Transducers and Piezoelectric Micromachined Ultrasonic Transducers. Details of their descriptions, fundamental principles and fabrication methods will be described in the later sections.

## 2.4 Capacitive Micromachined Ultrasonic Transducers

### 2.4.1 Introduction

Since 1954, electrostatic transducers have frequently been applied to sound wave excitation and detection [21]. The principle of transduction is the vibration of a thin plate as a result of electrostatic forces applied cross it [22]. The microphone is one of the most well known electrostatic transducers, which takes advantage of this mechanism to generate and detect sonic waves. With the development of silicon micromachined techniques in miniaturization capability, MEMS-based electrostatic transducers operating at high frequencies level are fabricated, which are known as CMUTs [23].

Nowadays, CMUTs can be made over a wide range of operational frequencies, which ranges from several kilohertz (kHz) up to one hundred megahertz (MHz) [16]. In the meantime, they can also be fabricated in even smaller scale with superior precision, as shown in Figure 2-2 [24]. These feasibilities provide a broad technology platform, which allows CMUTs to be applied to various applications.

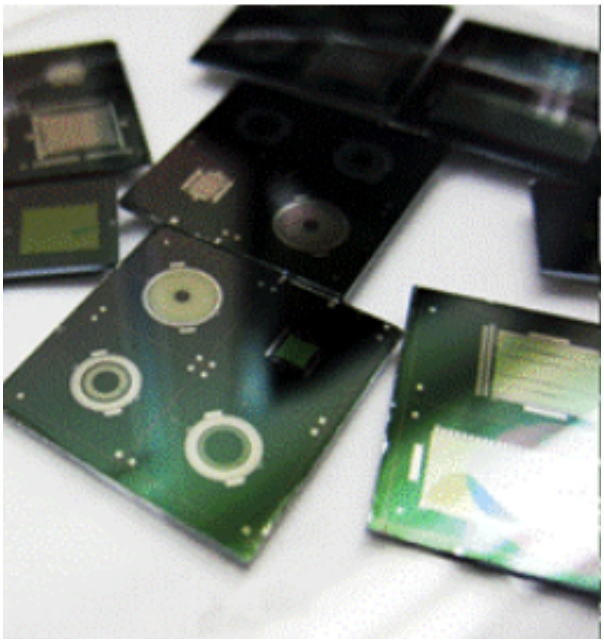

Figure 2-2 Optical picture of different CMUT design for various applications [24]

The first application of CMUTs introduced is air-coupled ultrasonic non-destructive testing (NDT) [25]. With the development of CMUTs, they can be used as air transducers as well as immersion transducers. Stanford University firstly proposed that CMUTs offer wider bandwidth

when operating in immersion, which can be used for bio-medical imaging [26]. Due to fabrication technologies, it can produce precise transducer arrays of CMUTs and miniaturized transducers for medical imaging. In particular, CMUTs fabrication process is compatible with complementary metal–oxide–semiconductors (CMOS) technology, since its process temperature can be controlled under 400°C [27][28][29]. This introduces a better integration level of CMUTs with supporting electronics, which improves device performance and packing. As a result, it becomes apparent that CMUTs are beneficial to medical imaging applications.

In addition to NDT and medical imaging, CMUTs can be applied to provide high-intensity focused ultrasound (HIFU) for therapeutic ultrasound applications as well [30]. They are designed to increase output pressures by using a narrow bandwidth. Furthermore, CMUTs can serve as sensors to measure physical dimensions and temperature of fluid in channels, when they are integrated into microfluidic channels for lab-on-a-chip applications [31].

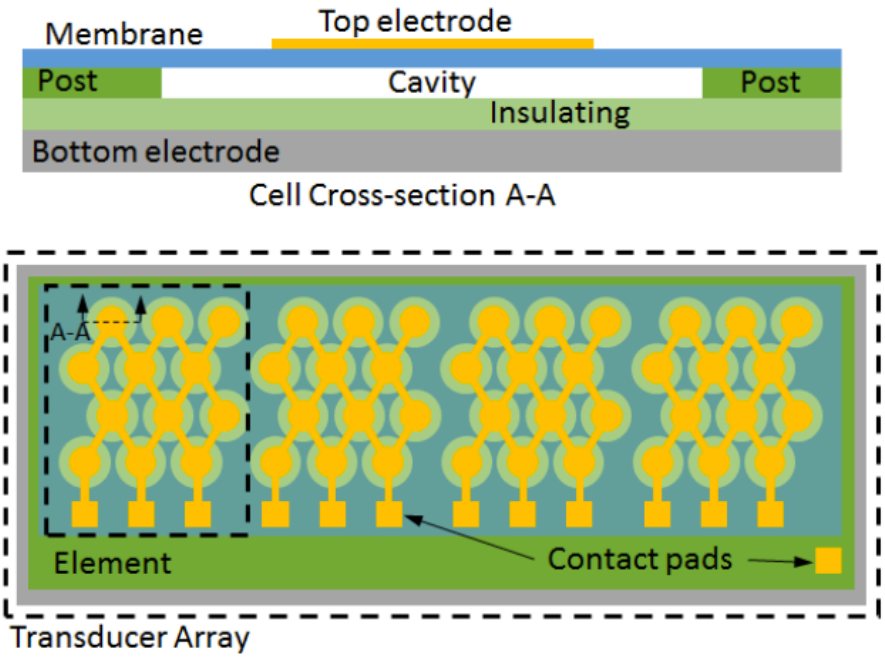


Figure 2-3 Illustration of basic CMUT structure [32]

CMUTs are the capacitive parallel-plate transducers that convert energy based on the change in capacitance. The fundamental structure of a CMUT is called a cell, as shown in Figure 2-3. Each cell basically consists of a membrane, a cavity, an insulating layer, a silicon substrate wafer, and top and bottom electrodes [22]. The small and thin membrane is suspended over a conductive silicon substrate

by an insulating support. The diameter of it ranges from 1μm to hundreds of micrometers. The cavity fabricated is vacuum-sealed or unsealed, whose thickness can be as small as 0.5μm. The metallized layer on the membrane acts as a top electrode, and a conductively doped silicon substrate can serve as a bottom electrode. There are three normal CMUT cells based on the different fabrication process, as shown in Figure 2-4. Type 1: When a membrane is conductive, no additional electrode is required, and then the membrane and the insulating material seal the cavity. Type 2 and 3: when a membrane is electrical insulated, an extra electrode is required, and either only the insulating layer or the insulating layer and the substrate can seal the cavity. When multiple cells have common electrodes, they become an element [32]. A CMUT array contains multiple elements with different electrodes as shown in Figure 2-3.

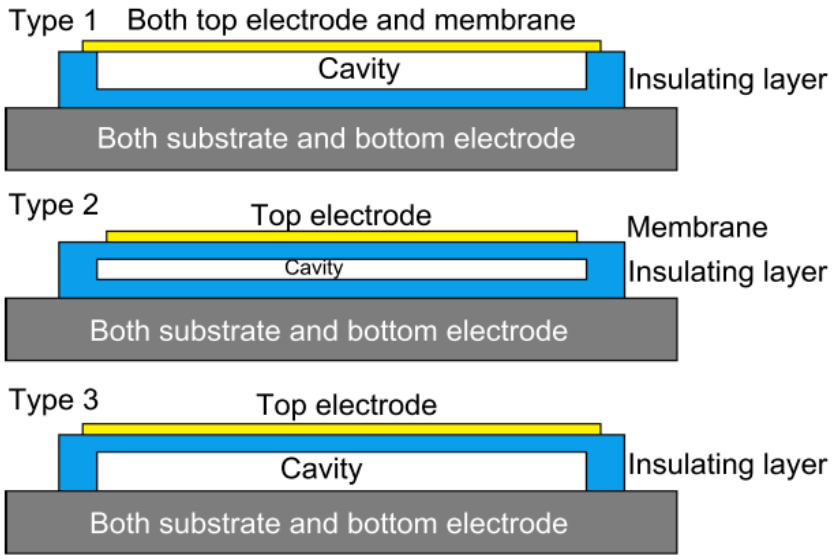


Figure 2-4 Three typical structures of CMUT cell

### 2.4.2 Fundamentals of Operation

The basic unit of a CMUT cell is a flexural mode plate, which is driven by electrostatic force. The structure of a CMUT with one moveable plate is essentially same as a parallel plate capacitor. One plate of the capacitor is the top electrode on the membrane. The conductive silicon substrate makes up the other plates of the capacitor [22]. When CMUTs are operated, they are biased with direct current

(DC) voltage. The membrane is deflected towards the bottom electrode by the electrostatic force [33]. At the same time, the residual force of material resists the deformation of the membrane. Under the transmit mode, if an alternating current (AC) voltage is applied to the device, then the membrane starts vibrating, thus the ultrasound could be generated. When the transducers are used as receivers, changes in pressure from the incoming ultrasonic waves cause the deflection of a membrane to induce capacitance to change and produce current, which can be measured [34]. It can be understood through the relationship between capacitance (C), charge (q), and voltage (V)

$$\mathrm{C} = \frac{q}{V}$$

The potential (V) is fixed due to the applied DC bias, as the capacitance changes with membrane vibration q must change correspondingly. A flow of electric charge between two electrodes with time, which means a current produced.

### 2.4.3 Fabrications of CMUTs

In general, CMUTs fabrication can be classified into two categories, which are surface micromachining technology, and wafer bonding technology. The main difference between these two techniques is how to optimize the formation of cavities and the properties of the membrane.

The surface micromachining of CMUTs fabrication has been developed for decades [32][35]. Each layer is deposited or patterned sequentially on the surface of a silicon substrate from bottom to top using thin-film depositions, thin-film etching, and photolithography, etc. [22]. A typical surface micromachining process is demonstrated in Figure 2-5.

The process starts with a silicon substrate. The bottom electrode is firstly deposited on the silicon substrate followed by an insulating layer, a sacrificial layer, membrane and top electrode. During the process of fabricating CMUTs, creating a cavity structure is one of the most important steps, which allows the membrane to vibrate. After the sacrificial layer deposition, releasing holes are patterned and etched on the sacrificial layer, which ensures that the sacrificial material can be removed by wet etching process. Then cavities can be achieved by releasing sacrificial layer. Cavities can be either sealed or not. If vacuum environment is required, another layer of insulating material will be deposited to seal releasing holes followed by top electrode deposition.

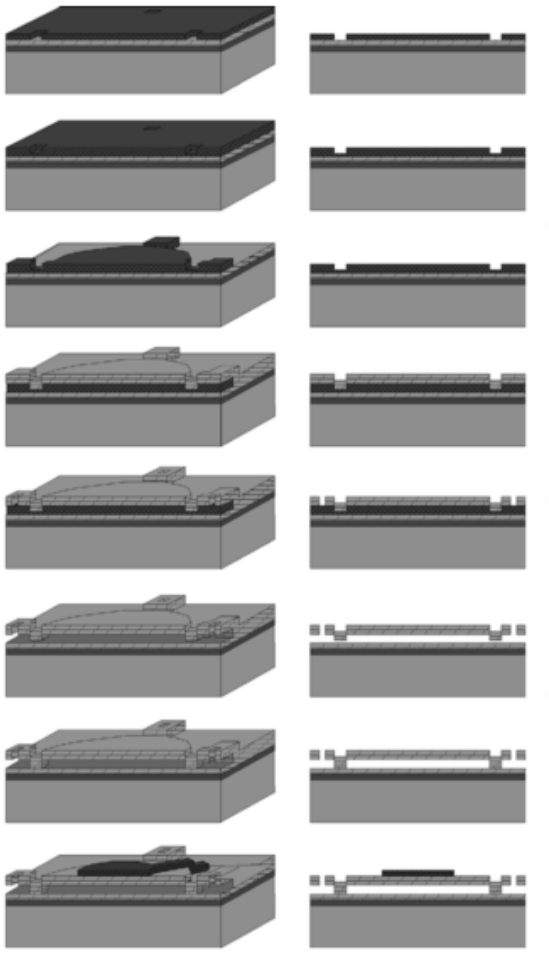

Figure 2-5 Surface micromachining fabrication process [32][35]

Surface micromachining process provides a straightforward method of CMUT fabrication. During this fabrication process, some factors should be considered such as fabrication efficiency, device performance and process controllability [32]. Therefore, multiple parameters need to be adjusted to achieve these requirements when designing CMUTs. For instance, material selection, the etchant type, and the basic structure of the CMUT cell. However, it is impossible to optimize all of these parameters at the same time. Furthermore, the existence of etching releasing holes and sacrificial layer also lead to some limitations. First of all, due to releasing holes patterned on the same layer with membranes, it decreases the fill factor that is the ratio of the CMUT area to the total aperture area [32][25][35]. A small fill factor gives rise to a low output power and sensitivity [32]. Second, other pattern and long time etching process may result in potential problems of CMUTs for

examples, sticking problem between membranes and substrate, uniformity of the layer as well as the thickness of membrane and cavity depth.

Another significant technique of fabricating CMUTs is the wafer bonding technology. It was firstly illustrated by Huang *et al*. in 2003 [36]. The conventional wafer bonding process is depicted in Figure 2-6. It involves two wafers, one for the top wafer and another one for the bottom wafer [32][37]. The typical bottom wafer is usually a highly doped silicon wafer. The top wafer is a silicon-on-insulator (SOI) wafer, which serves as a membrane. After growing an insulation layer on the bottom wafer, cavities are patterned by photolithography and etching process. Then membrane layer is directly attached on cavities through wafer bonding technique in a vacuum environment. When the top and bottom wafers are brought into contact, molecular bonds can be generated between two wafers forming strong bonds. These bonds can become inseparable if a subsequent high-temperature annealing process is executed. The final step is to release membrane and pattern electrodes.

This fabrication process provides several advantages over surface micromachining technique [32][37]. Wafer bonding method is much simpler to control. It does not require releasing holes for cavities, which improves the active area of CMUT. However, this technique typically needs high operational temperature during the annealing process, which is hard to be integrated with CMOS fabrication. Besides, it requires that the wafers' surface roughness is highly uniform, which is commonly achieved by either using very expensive SOI wafers or polishing wafer through chemical mechanical polishing (CMP) process.

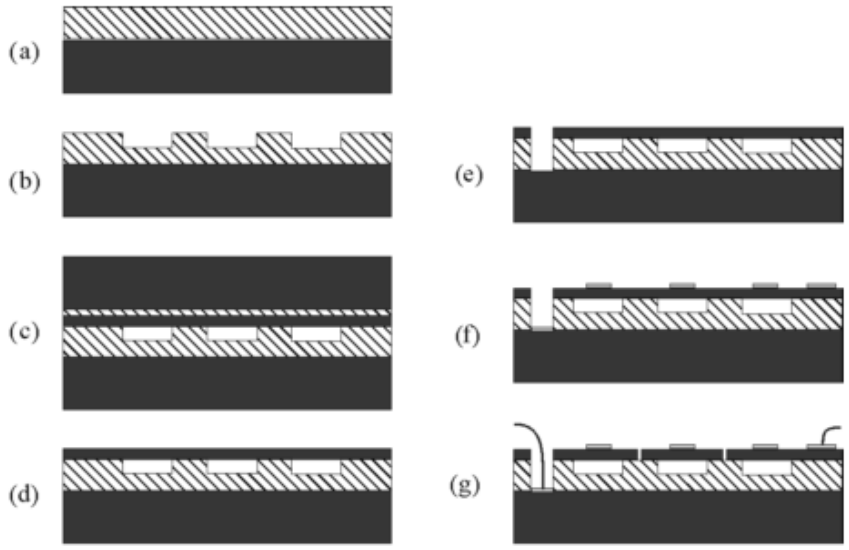


Figure 2-6 Wafer bonding fabrication process [37]

## 2.5 Piezoelectric Micromachined Ultrasonic Transducers

### 2.5.1 Introduction

Piezoelectric Micromachined Ultrasonic Transducers (PMUTs) are another type of MUTs. According to the previous studies, piezoelectric thin film structures have been found in a wide variety of MEMS devices for ultrasonic transducers. For example, the lead zirconate titanate (PZT) film has a conventional structure because of its high piezoelectric constant, high energy density and high electric-mechanical coupling coefficient, which can serve as an actuating or sensing component in a transducer [38]. Current ultrasonic transducers are usually referred to as conventional ultrasonic transducers, which consist of a PZT film sandwiched by two electrodes as shown in Figure 2-7 (a).

PMUTs are considered as the micromachined resonators with a multi-layered membrane, which introduces a new approach for ultrasonic transducers [39][40][41][42]. They have a similar structure to CMUTs, as shown in Figure 2-7 (b). An essential PMUT structure is composed of a piezoelectric layer clamped by a top and a bottom electrode on a structural layer [39]. Both of them are parts of a movable membrane. Besides, a cavity is not required between two electrodes in PMUT structure. Comparing with the conventional PZT ceramic based ultrasonic transducers whose resonance frequency highly depends on the dimensions and properties of the piezoelectric layer, the resonance

frequency of PMUTs is controlled by the dimensions and properties of the structural layer rather than the piezoelectric layer.

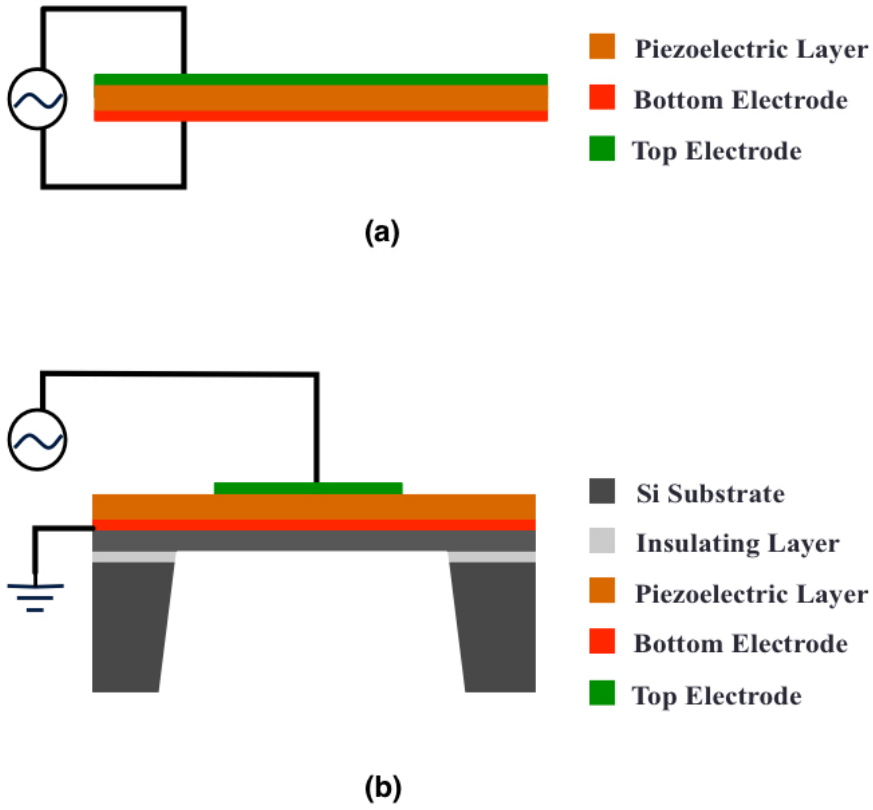


Figure 2-7 Illustration of basic structure (a) conventional ultrasonic transducers (b) PMUTs

### 2.5.2 Fundamentals of Operation

Comparing with CMUTs, PMUTs operate under the mechanism of piezoelectric effect instead of electrostatic transduction. The piezoelectric effect is a specific property of the materials, which can generate an electric charge in response to applied mechanical stress. This effect is reversible, which exhibits to two terms: the direct piezoelectric effect and the inverse piezoelectric effect. When a mechanical stress is applied to a substrate, it produces an electric charge. Conversely, a mechanical deformation is produced when an electric field is applied.

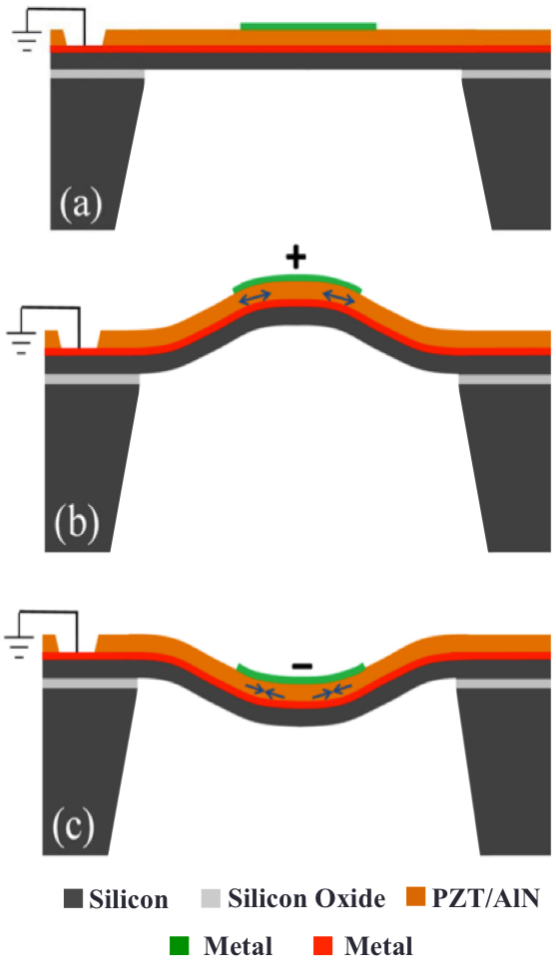


Figure 2-8 Schematic diagram of PMUTs' fundamental operation

PMUTs can be operated as both transmitters and receivers based on the piezoelectric effect, as shown in Figure 2-8. As a transmitter, an electric field applied between the top and bottom electrodes induces a transverse stress on the piezoelectric layer [43]. Since the edge of the piezoelectric layer is clamped, the generated stress creates a bending moment mismatched between the piezoelectric layer and structural layer, which forces the membrane to deflect and create sound wave into the surrounding medium. As a receiver, due to the coming sound wave, an incident stress deflecting the plate causes a charge on electrodes, which can be amplified and detected.

### 2.5.3 Fabrications of PMUTs

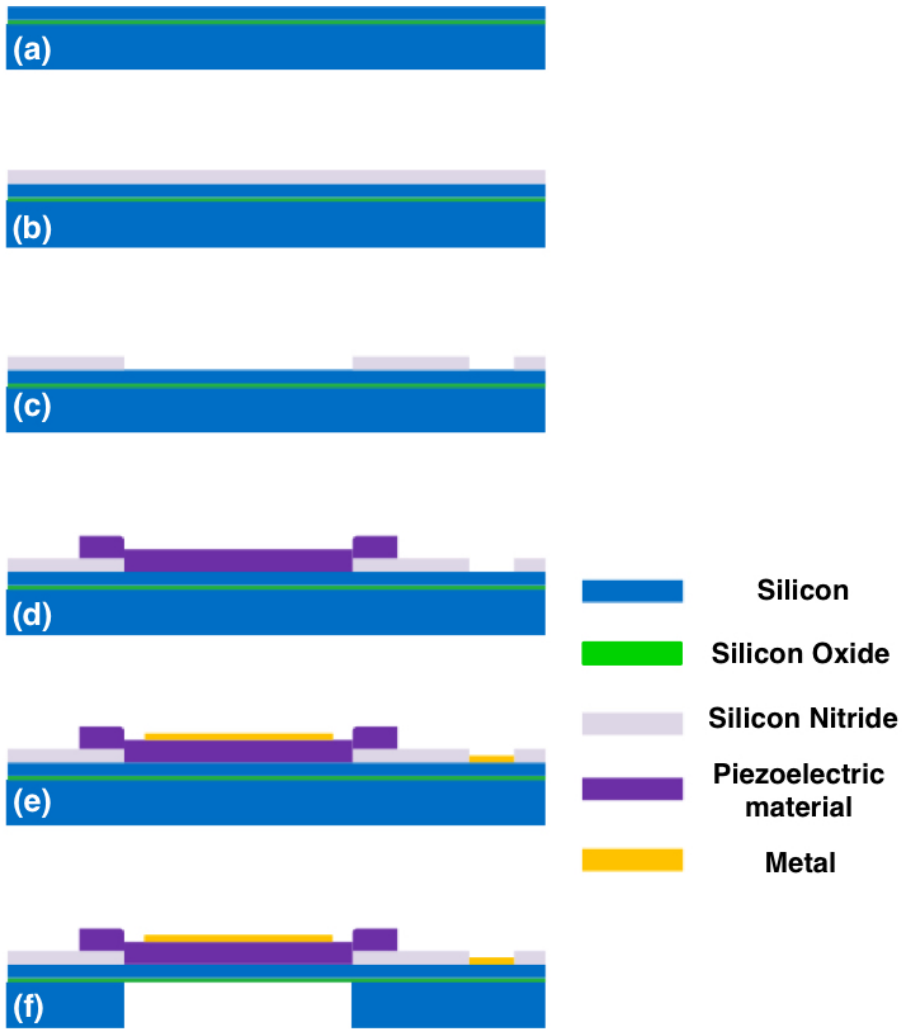


Figure 2-9 A fabrication flow of PMUTs

PMUTs can be fabricated by several different methods based on the surface micromachining technique. The back-side etching is the most conventional method for fabricating PMUTs [44]. It can be performed either before deposition of the piezoelectric layer [44][45] or after completing the whole membrane building [39][44][46]. The small difference of the sequence is mainly depends on the initial substrate and the etching stop layer. In many early PMUTs, a single-crystal silicon wafer is used as the initial substrate, and a boron-doped Si is an effective etching stop layer. Alternatively, the

SOI wafer with a buried oxide layer that is used as an etching stop is widely applied to PMUTs fabrication as well.

A typical fabrication flow of PMUTs is shown in Figure 2-9. In this fabrication process, the first step (step a) is to prepare a SOI wafer with a tailored thickness of device layer that acts as a structural layer of PMUTs. The thickness of device layer should be taken into account, since it is critical to the resonance frequency as mentioned before. A highly doped device layer with higher conductivity is desired, which can also be used as a bottom electrode. Otherwise, an additional bottom electrode deposited on device layer is needed. Then, a layer of silicon nitride is deposited and serves as the insulating layer (step b). After patterning (step c), a piezoelectric layer is deposited by reactive sputtering (step d). There are three most common piezoelectric materials that are zinc oxide (ZnO), PZT, and AIN [39]. The next step (step e) is the deposition of the top electrodes and metal pads. Based on the theoretical and particle studies, the optimal coverage of a top electrode over a structural layer on PMUTs is 60% [47]. In the final step, the dimension of a PMUT cell is defined by back-side etching through DRIE process.

## 2.6 Discussion

Based on the previous studies of many researchers, CMUTs and PMUTs display many advantages for gas sensing.

First of all, initial researches of MEMS resonant chemical sensors such as QCM and SAW have proved good performances for gas sensing. While, when these devices are implemented as arrays for gas sensing, the size of transducers is still large [16]. The CMUTs and PMUTs based on MEMS fabrication technology have been actively explored to further reduce the dimensions as chemical sensors.

Second, for CMUTs, they can be fabricated in the form of a vacuum cavity structure, which results in a higher quality factor (Q) than MEMS beams to reduce the overall energy loss and improve sensor resolution [16]. Q is a key parameter of MEMS resonators. It indicates that the rate of energy loss relatives to the stored energy of a resonator. It also decides the resolution of chemical sensors, which demonstrates how selective the transducers are around resonance frequency [16].

Third, CMUTs can be easily composed of elements in the form of a 1D or 2D array. In one CMUT element, there are tens to hundreds of CMUT cells connected in parallel, which enhance the sensing area and the reliability of a single-resonator system.

Forth, a repeatable and reliable MEMS fabrication process of CMUTs and PMUTs reduces their cost and ensures a single resonance frequency in air.

Moreover, comparing the CMUTs and PMUTs. CMUTs requires additional bias voltage except for alternating current signal and have the dielectric charging effect problem due to its structure, which should be considered for gas sensor. PMUTs are actuated only by an AC signal, which is easier to be integrated with the low power oscillation circuit.

# Chapter 3
# Principle of Operation for Gas Sensing

## 3.1 Mass-loading Effect

The fundamental sensing mechanism of CMUTs and PMUTs is the mass-loading effect. The diagram describes the flow of how resonant chemical sensors based on the gravimetric method (mass-loading effect) are used for gas sensing, as shown in Figure 3-1. The gas with a concentration attached on the sensing layer results in a mass change of resonant structure, which causes a shift of its resonance frequency. Then, the motion (displacement, rotation, strain) of the resonators is converted into an electrical signal by different transduction such as capacitive, piezoelectric or piezoresistive mechanism [48][49]. This signal at the shift frequency is amplified and phase shift to satisfy the self-vibration conditions of a resonator. An actuation force of electrostatic or piezoelectric origin then transmits the signal into the resonator again.

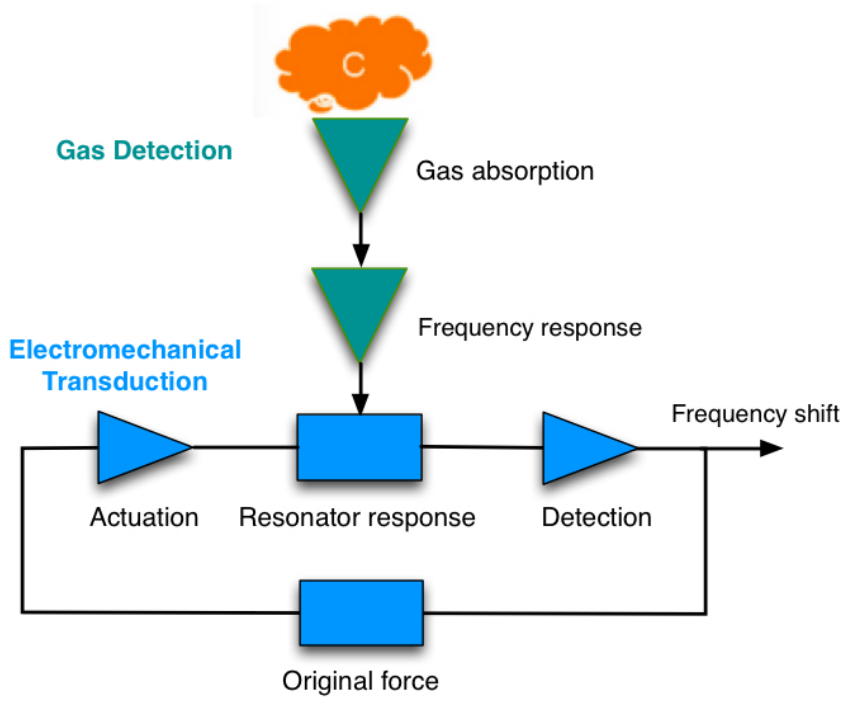


Figure 3-1 General topology of gas sensors based on the gravimetric method [49]

In the case of CMUTs or PMUTs, the additional mass of chemical analyte loaded on a functionalized resonant structure (membrane) results in a shift of its resonance frequency that can be

measured continuously. The Figure 3-2 shows a schematic diagram of operational principle for gas sensing by frequency shift measurement. The X-axis is “frequency," while the Y-axis is “Magnitude." The blue line in the diagram indicates the initial spectrum where the membranes are deposited with sensing film. After gas attaches on the sensing film, the frequencies decrease, so that the blue line shifts to left. The mass loading is induced by the gas absorption in the sensing layer (for example polymers) covered with the membrane. Knowing the chemical affinity of the sensing layer with gas molecules, then the frequency shift can be related to the gas concentration [49].

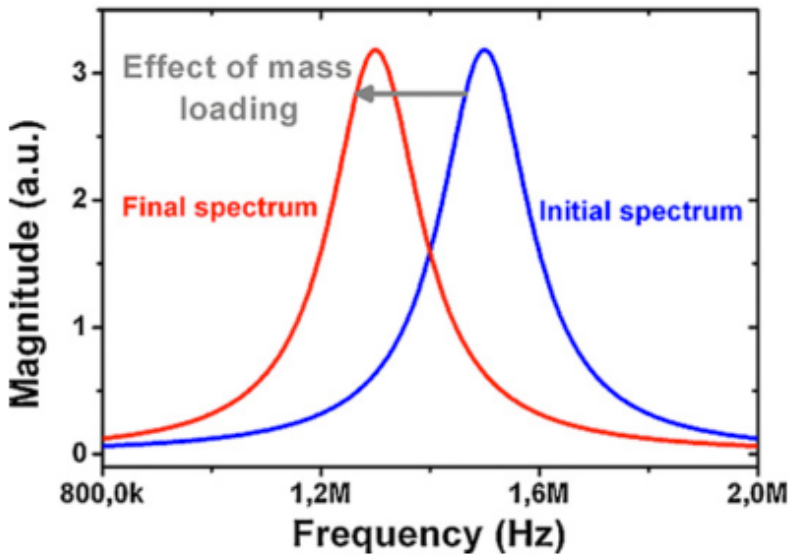


Figure 3-2 Schematic diagram of operational principle for gas sensing by frequency shift measurement [49]

# Chapter 4
# Development of PMUTs and CMUTs for Gas Sensing

In the previous chapter, the potential of using CMUTs and PMUTs as resonant chemical sensors were presented and explained. This chapter specifically demonstrates how CMUTs and PMUTs work for ethanol detection, which is the core of this thesis. It starts with a description of the transducers applied for gas sensing with details. The resonance frequency in another word the fundamental frequency can be calculated based on the theory of vibration plate. Then the mass-loading effect is taken into considerations in Finite Element Method (FEM) Model.

## 4.1 Device Description

The purpose of this thesis is to prove the viability of CMUTs and PMUTs as resonant chemical sensors for ethanol detection. Existing CMUTs and PMUTs fabricated by our lab are used instead of designing new transducers. There are four case studies in the research. The first two case studies use PMUTs with resonance frequency at 600kHz and 2.3MHz in air separately. The last two case studies use CMUTs designed initially for the medical imaging application. The CMUTs for medical imaging always operate at several megahertz or higher frequency. The resonance frequencies of the CMUTs used are 4.56Mhz and 6.4MHz in air.

Table 4-1 Structural dimension of the PMUTs

| | Case study 1: PMUTs | Case study 2: PMUTs |
|---|---|---|
| Piezoelectric layer dimension (μm) | 260 | 220 |
| Piezoelectric layer thickness (μm) | 0.5 | 0.5 |
| Silicon layer dimension (μm) | 500 | 220 |
| Silicon layer thickness (μm) | 10 | 10 |
| Insulating layer thickness (μm) | 1 | 1 |
| Electrode dimension (μm) | 240 | 100 |
| Electrode thickness (nm) | Cr 20 Al 1000 | Cr 20 Al 1000 |

In the first two studies, the PMUTs structures were designed in square-shaped with different structural dimensions as shown in Table 4-1. The Figure 4-1 shows a top view of the PMUTs and a cross-section schematic of a PMUT cell. The bigger size of square cells was designed for lower resonance frequency, while the smaller size of square cells was designed for higher frequency.

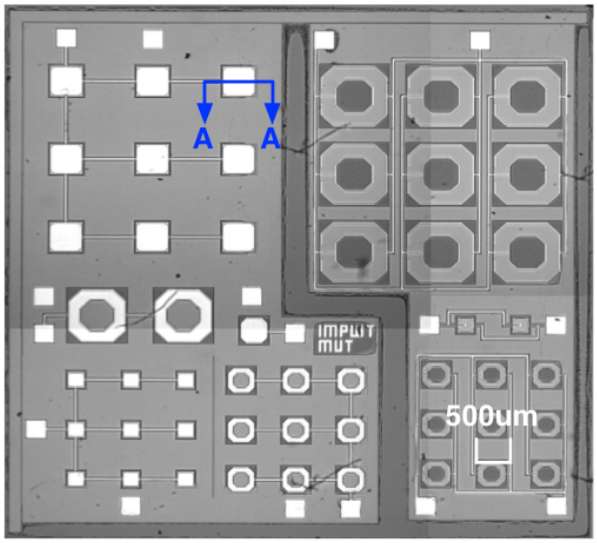


(a)

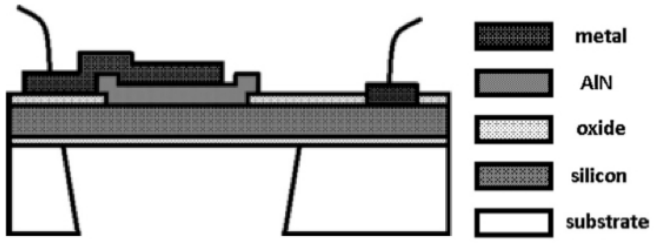


A-A cross-section schematic

(b)

Figure 4-1 (a) Top view of PMUTs with different dimensions (b) Cross-section schematic of a single PMUT cell [39]

These PMUTs were fabricated by using multi-user MEMS process (MUMPs) that is a SOI based surface micromachining technique. Besides, it is a commercially available fabrication process, which

provides a low cost and accessible option for MEMS researchers [39]. A brief description of the PMUTs fabrication process is illustrated, which is helpful to visualize the PMUT structure.

It began with a SOI wafer including a silicon device layer, an oxide layer, and a substrate [39]. The silicon layer was doped and served as the bottom electrode of PMUT. Then another oxide layer was grown on the doped silicon, which provides an insulation layer between the top electrode and bottom electrode. The next step was the deposition of the piezoelectric layer by sputtering. Aluminum Nitride (AIN) was chosen as the piezoelectric material because of its higher receive sensitivity. After that, a layer of chromium and a layer of aluminum were deposited on AIN as top electrodes and bond pads. The final step was the membrane-releasing process by DRIE through the substrate from the bottom side of SOI wafer. For PMUTs, the vibrational membrane is composed of doped silicon, AIN, and metals that are the bottom electrode, piezoelectric layer, and top electrode respectively.

In case study 3, the first generation of CMUTs fabricated by polymer wafer bonding technique in our lab was applied to gas sensing. Both of the CMUT cells in case study three and four were designed in circular shape, which is different from PMUTs. The structural dimensions of the 1st generation CMUTs are shown in Table 4-2 [32].

Table 4-2 Structural dimensions of the 1st generation CMUTs (Case study 3) [32]

| | |
|---|---|
| Membrane diameter (μm) | 50 |
| Membrane thickness (nm) | 605 |
| Cavity depth (nm) | 378 |
| Insulating layer thickness (nm) | 1059 |
| Top electrode diameter (μm) | 25 |
| Top electrode thickness (nm) | Cr 30 and Al 65 |

The Figure 4-2 is a visual description of the CMUTs [32]. The membrane is LPCVD silicon nitride (SiN) with the thickness of 605μm and diameter of 50μm. The top electrode with the diameter of 25μm is a part of the movable membrane, which includes a layer of chromium (Cr) with the thickness of 30μm and a layer of aluminum (Al) with the thickness of 65μm. The Cr layer is to promote adhesion between SiN and Al. A doped silicon wafer is used as the bottom electrode, which is separated from the membrane by a vacuum cavity with the depth of 378nm. The insulating layer consists of two layers of photo BCB bonded together with the thickness of 1059nm in total.

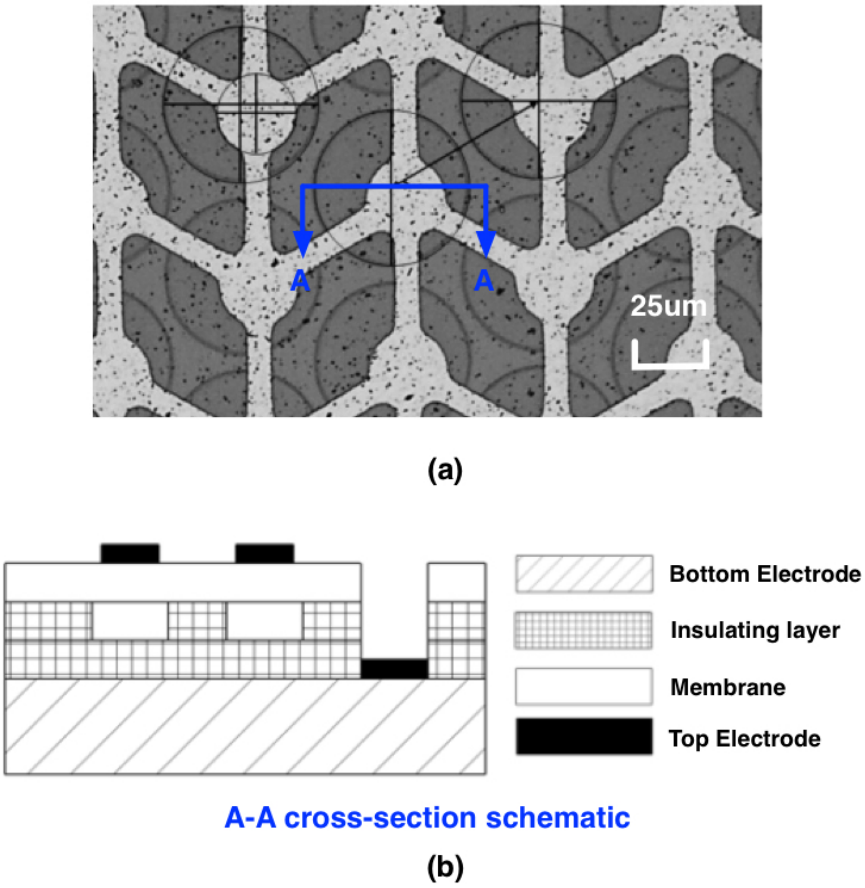


Figure 4-2 (a) Microscopy image of the 1st generation CMUTs (Case study 3) (b) Cross-section schematic of a single CMUT cell [32]

The CMUTs were fabricated by polymer wafer bonding technique, which is a simpler fabrication process comparing with surface micromachining technique. The fabrication flow is shown in Figure 4-3 [32]. It started with two silicon wafers (top and bottom wafers). The top wafer was a boron-drop silicon wafer with a SiN layer deposited by LPCVD process, and the bottom wafer was another boron-drop silicon wafer acting as the bottom electrode. They firstly cleaned by RCA-1 that a procedure for removing residue and films from wafers (step 1-a and step 1-b) [32][50]. Photo BCB (Cyclotene 4000 series, Dow Chemical) was deposited on both of the wafers by spin coating (step 2-a and step 2-b). Then, some works such as backing and exposing under UV light were done to prepare to bond. After patterning cavities on the top wafer by photolithography (step 3), both of the top and bottom wafers were soft cured for an hour in a vacuum oven at 190°C. Then, these two wafers were bonded together by mechanical clamps in the vacuum chamber under a compressive pressure of

0.4MPa (step 4). The BCB full curing process was proceeding in the meanwhile. The top and bottom wafers were firstly heated up to 150°C and maintained for 15 minutes. Then, the temperature was increased to 250°C and kept for an hour. After that, the nitrogen gas flow was used to cool down these two wafers until the temperature decreases to 150°C. The next was the membrane-releasing step (step 5). The silicon substrate of the top wafer was removed by wet etching using KOH (25% concentration at 70°C for 12 hours). The last three steps were depositions of top electrodes and bonding pads by e-beam lift-off process (step 6-8).

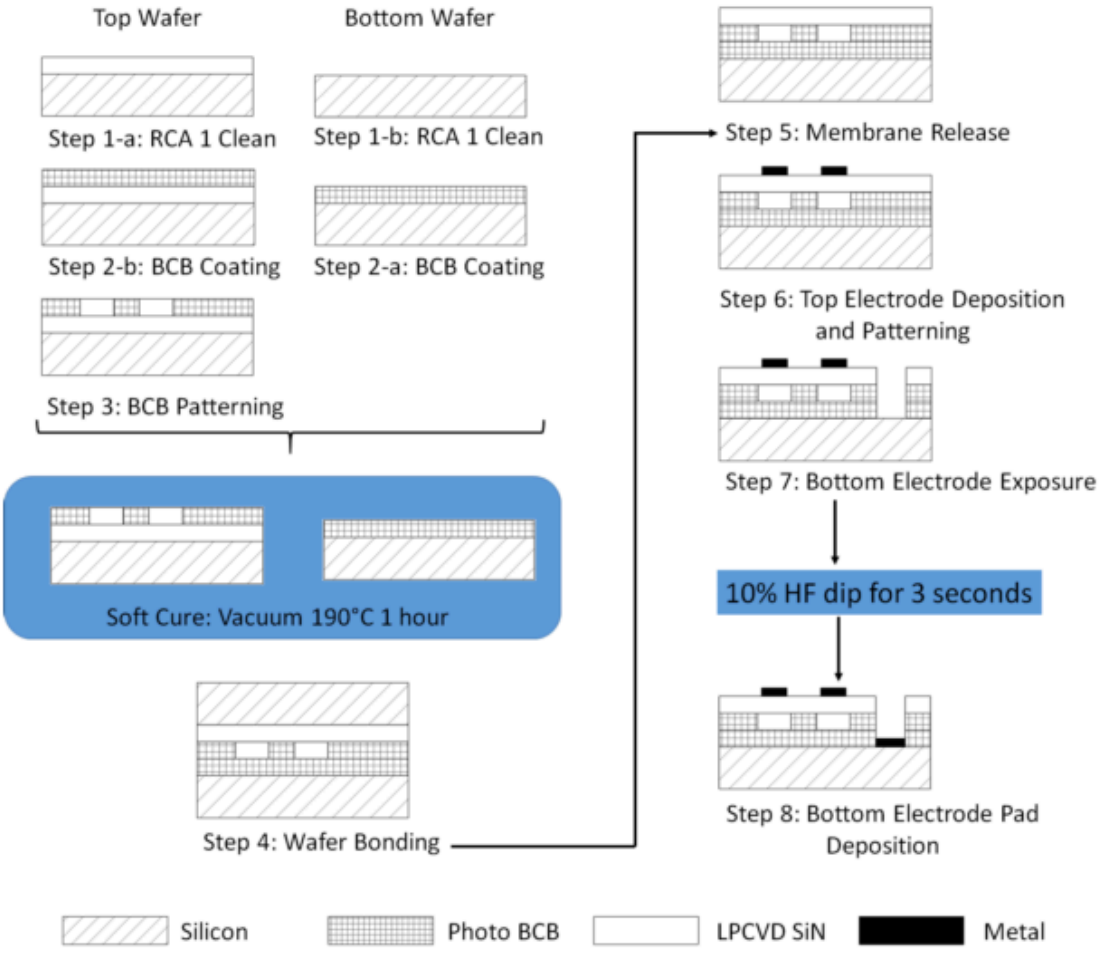


Figure 4-3 Fabrication flow of the 1st generation CMUTs (Case study 3) by polymer wafer bonding technique [32]

Although this method shows a simpler fabrication process, there are some limitations [32]. For example, the thickness of the cavity depth and the insulating layer is depended on the thickness of the

BCB adhesive layers. Since the spin rate of the spinner used is limited to 7000RPM, and there is no difference in coating thickness but in uniformity of BCB by varying the spin rate higher than 5000RPM. It is hard to decrease the thickness of cavity depth and the insulating layer by controlling the thickness of BCB layer.

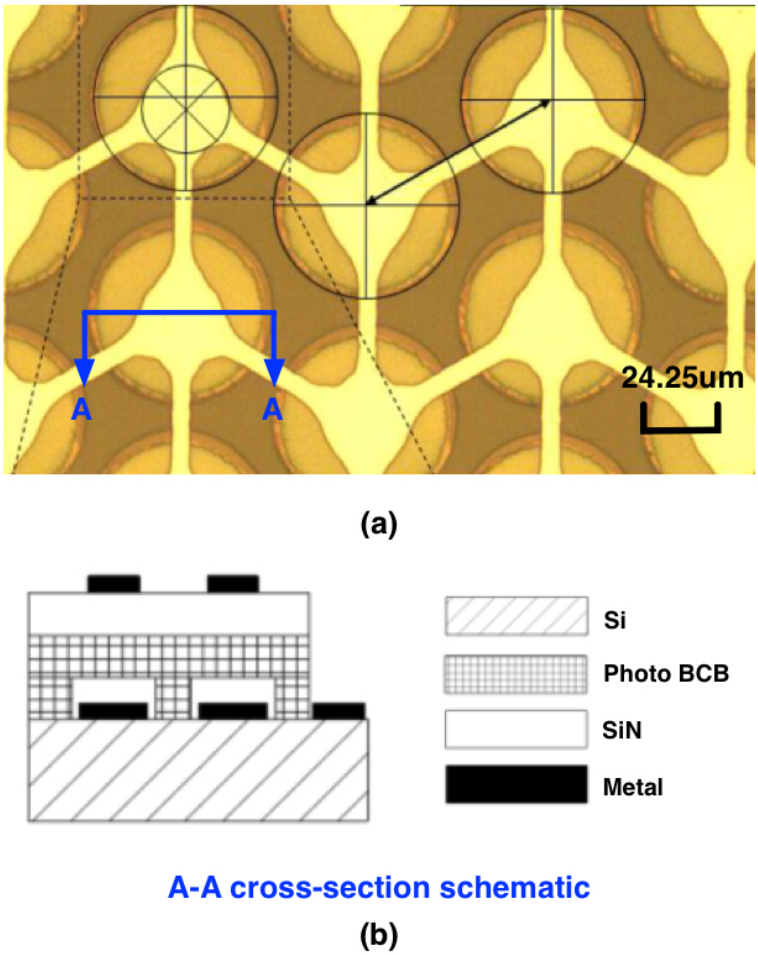


Figure 4-4 (a) Microscopy image of the 2nd generation CMUTs (Case study 4) (b) Cross-section schematic of a single CMUT cell [32]

In case study 4, the second generation BCB CMUTs with higher resonance frequency was used for ethanol detection. The structure of 2nd generation CMUTs is similar to the first generation, as shown in Figure 4-4. The main difference is that the membrane layer of the 2nd generation CMUTs consists of two materials: LPCVD SiN and photo BCB. Furthermore, additional metal layers

deposited inside the cavities are used as a part of bottom electrodes. The variations of the structure of 2nd generation CMUTs are sufficient to simplify and control the fabrication process.

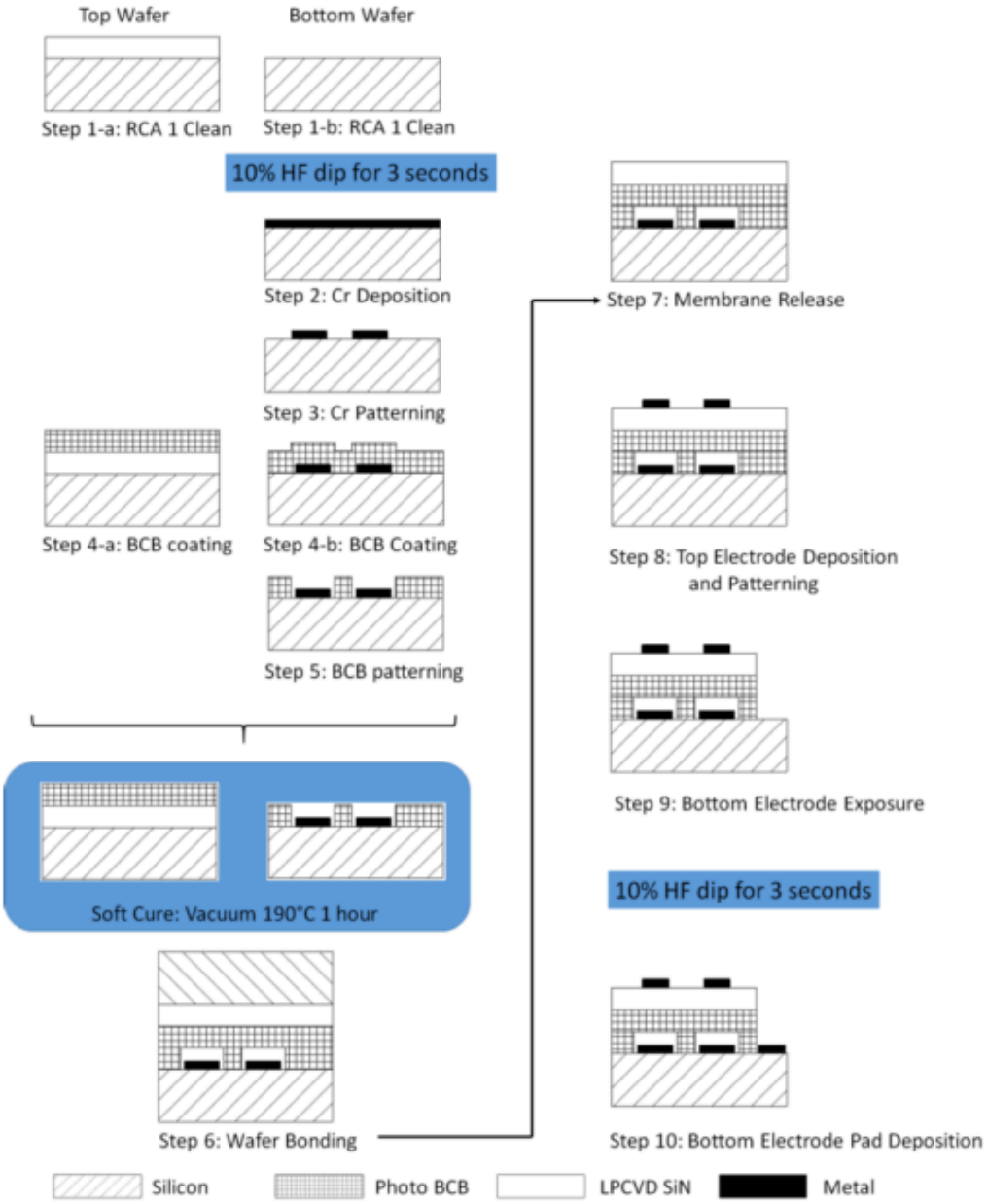


Figure 4-5 Fabrication flow of the 2nd generation CMUTs (Case study 4) by polymer wafer bonding technique

The shows the fabrication flow of 2nd generation BCB CMUTs. The detailed processes of BCB coating and patterning, wafer bonding, and top electrodes and electrical pads deposition were same as described in the 1st generation CMUTs fabrication [32]. Comparing with the 1st generation CMUTs fabrication process, in the 2nd generation CMUTs fabrication process, the cavities were patterned on

the bottom wafer rather than the top wafer. After RCA-1 cleaning, the bottom wafer was dipped in 10% HF for 3 seconds (step 1-b). Then a layer of Cr was sputtered on the bottom wafer and patterned as bottom electrodes by photolithography and wet etching (step 2-3). The BCB layers were spin-coated on both of wafers (step 4) before patterning cavities and exposing Cr pads on the bottom wafer (step 5). The next steps, such as polymer wafer bonding, top electrodes, and wire bonding pads deposition follows the same recipes of those used in 1st generation.

Table 4-3 Structural dimensions of the 2nd generation CMUTs (Case study 4) [32]

| | |
|---|---|
| Membrane diameter (μm) | 48.5 |
| Membrane layer 1 (SiN) thickness (nm) | 605 |
| Membrane layer 2 (BCB) thickness (nm) | 1311 |
| Cavity depth at wafer center (nm) | 305 |
| Top Electrode diameter (μm) | 23.5 |
| Top Electrode thickness (nm) | Cr 30 and Al 65 |
| Bottom electrode diameter (μm) | 45.3 |
| Bottom electrode thickness (nm) | 30.5 |

In summary, the most significant feature of the 1st and the 2nd generations of CMUTs is their fabrication process that uses polymer wafer bonding technique. Comparing with conventional fabrication techniques (surface micromachining and wafer bonding), it uses the polymer wafer instead of the SOI wafer, which is low cost. Besides, it is a low-temperature process, which enables integrate CMUT gas sensors with ICs. The entire process requires only lithography tools, metal deposition tools, and wafer bonding tools, which simplifies fabrication difficulties. The polymer wafer bonding also has good tolerance to contaminations and wafer defects, so it does not require high-level clean room. It provides an alternative method for fabricating CMUTs in future.

## 4.2 Figure of Merit (FOM)

### 4.2.1 Resonance Frequency

The resonance frequency is referred to as the fundamental frequency, which is identified by the physical parameters of the vibrating object. According to Rayleigh-Ritz method, the fundamental

frequency of a thin isotropic plate can be determined by solving the characteristic equation shown below [51]:

$$|K - \omega^2 M| = 0 \qquad \text{Equation 1}$$

,where

$$K = \begin{bmatrix} k_{11} & L & k_{1n} \\ \text{M} & & \text{M} \\ k_{n1} & L & k_{nn} \end{bmatrix}$$

$$M = \begin{bmatrix} m_{11} & L & m_{1n} \\ \text{M} & & \text{M} \\ m_{n1} & L & m_{nn} \end{bmatrix}$$

$$k_{ij} = k_{ji} = \iint_S D\left\{(\nabla^2 \emptyset_i)(\nabla^2 \emptyset_j) - (1-\mu)\left(\frac{\partial^2 \emptyset_i}{\partial x^2}\frac{\partial^2 \emptyset_j}{\partial y^2} + \frac{\partial^2 \emptyset_i}{\partial y^2}\frac{\partial^2 \emptyset_j}{\partial x^2} - 2\frac{\partial^2 \emptyset_i}{\partial x \partial y}\frac{\partial^2 \emptyset_j}{\partial x \partial y}\right)\right\} dx\, dy$$

$$m_{ij} = m_{ji} = \iint_s \rho h \emptyset_i \emptyset_j \, dx\, dy, \;\; i, j = 1, 2, \cdots, n$$

$$D = \frac{Eh^3}{12(1-\mu^2)}$$

$$\nabla^2 = \left(\frac{\partial^2}{\partial^2 x} + \frac{\partial^2}{\partial^2 y}\right) \qquad \text{Equation 2}$$

$\emptyset_i, i = 1, 2, \cdots, n$ is the assumed *i*th vibration mode, which satisfies the boundary conditions. *S* is the surface area of the plate. *D* is the flexural rigidity, which is determined by the physical properties of the plate. *E* is the Young's Modulus of the plate material, *h* is the plate thickness, $\rho$ is the density of the plate material, and $\mu$ is the poison's ratio.

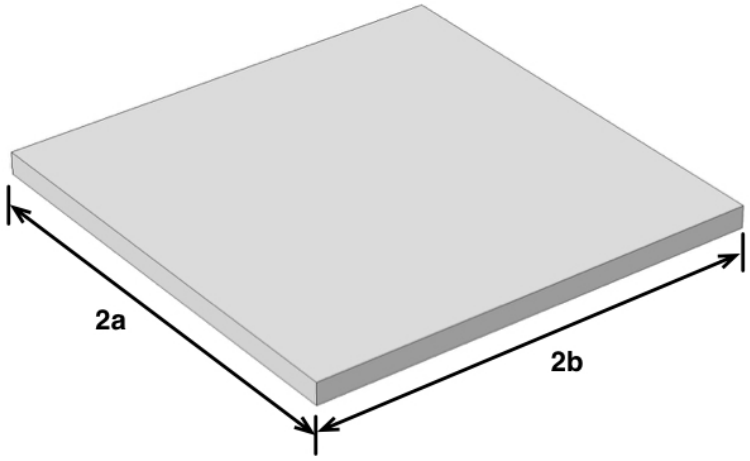


Figure 4-6 A square plate

For a clamped rectangular plate, as shown in Figure 4-6, $\emptyset_i$ is supposed to satisfy the following the displacement conditions:

$$\emptyset_i(a,b) = 0, \emptyset_i(-a,b) = 0$$

$$\emptyset_i(-a,-b) = 0, \emptyset_i(a,-b) = 0 \qquad \text{Equation 3}$$

, and the velocity conditions:

$$\left.\frac{\partial \emptyset_i(x,y)}{\partial x}\right|_{x=a} = 0, \left.\frac{\partial \emptyset_i(x,y)}{\partial x}\right|_{x=-a} = 0$$

$$\left.\frac{\partial \emptyset_i(x,y)}{\partial y}\right|_{y=b} = 0, \left.\frac{\partial \emptyset_i(x,y)}{\partial y}\right|_{y=-b} = 0 \qquad \text{Equation 4}$$

With the displacement conditions and the velocity conditions, $k_{ij}$ in Equation 2 can then be satisfied as:

$$k_{ij} = \iint_S D(\nabla^2 \emptyset_i)\left(\nabla^2 \emptyset_j\right) dx\, dy \qquad \text{Equation 5}$$

Now, choosing the *i*th (*n*=1) modal vibration mode as:

$$\emptyset_1(x,y) = (x^2 - a^2)^2 (y^2 - b^2)^2 \qquad \text{Equation 6}$$

, which can be proved to satisfy the conditions of Equation 3 and Equation 4. Taking Equation 6 into Equation 5 yields:

$$k_{11} = \iint_S D(\nabla^2 \emptyset_1)^2 \, dx \, dy = 2\int_0^a 2\int_0^b D(\nabla^2 \emptyset_1)^2 dx \, dy = \frac{2^{15}D}{3^2 \times 5^2 \times 7}\left(a^4 + b^4 + \frac{4}{7}a^2b^2\right)a^5b^5$$

Equation 7

, and

$$m_{11} = \iint_S \rho h \emptyset_1^2 \, dx \, dy = 2\int_0^a 2\int_0^b \rho h \emptyset_1^2 \, dx \, dy = \frac{2^{16}\rho h}{3^4 \times 5^2 \times 7^2}a^9b^9$$

Equation 8

By submitting Equation 7 and Equation 8 into Equation 1, the fundamental angular frequency of a clamped rectangular plate can be derived as:

$$\omega = \frac{\sqrt{\frac{63}{2}\left(1+\frac{4a^2}{7b^2}+\frac{a^4}{b^4}\right)}}{a^2}\sqrt{\frac{D}{\rho h}} \qquad \text{Equation 9}$$

For a square plate where $a$=$b$, then the fundamental angular frequency is:

$$\omega = \frac{9}{a^2}\sqrt{\frac{D}{\rho h}} \qquad \text{Equation 10}$$

At the mean time, $k_{ij}$ and $m_{ij}$ can also be rewritten regarding polar coordinates:

$$k_{ij} = 2\pi \int_s D\left(r\frac{d^2\emptyset_i}{dr^2}\frac{d^2\emptyset_j}{dr^2} + \frac{1}{r}\frac{d\emptyset_i}{dr}\frac{d\emptyset_j}{dr}\right)dr \qquad \text{Equation 11}$$

$$m_{ij} = 2\pi \int_s \rho h \emptyset_i \emptyset_j r dr \qquad \text{Equation 12}$$

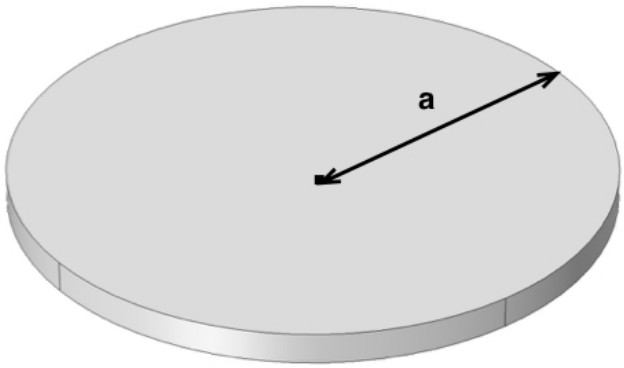


Figure 4-7 A circular plate

For a clamped circular plate, as shown in Figure 4-7, $a$ is the radius. Assuming the $i$th modal vibration mode as:

$$\emptyset_i(r) = \left(1 - \frac{r^2}{a^2}\right)^{i+1}, i = 1, 2, 3, \cdots, \mathrm{n} \qquad \text{Equation 13}$$

, which can be proved to satisfied fixed boundary conditions of Equation 3 and Equation 4. If $n$ is taken as 2, then having:

$$K = \begin{bmatrix} \frac{64}{3a^2}\pi D & \frac{16}{a^2}\pi D \\ \frac{16}{a^2}\pi D & \frac{96}{5a^2}\pi D \end{bmatrix},$$

$$M = \begin{bmatrix} \frac{\pi}{5}\rho h a^2 & \frac{\pi}{6}\rho h a^2 \\ \frac{\pi}{6}\rho h a^2 & \frac{\pi}{7}\rho h a^2 \end{bmatrix} \qquad \text{Equation 14}$$

Therefore, by taking Equation 14 into Equation 1, the following characteristic equation can be defined as:

$$\begin{vmatrix} \frac{64}{3} - \frac{\lambda}{5} & 16 - \frac{\lambda}{6} \\ 16 - \frac{\lambda}{6} & \frac{96}{5} - \frac{\lambda}{7} \end{vmatrix} = 0 \qquad \text{Equation 15}$$

, where

$$\lambda = \omega^2 a^4 \rho h/\mathrm{D} \qquad \text{Equation 16}$$

By solving Equation 15, the fundamental angular frequency of a clamped circular plate is,

$$\omega = \frac{10.21}{a^2}\sqrt{\frac{D}{\rho h}} \qquad \text{Equation 17}$$

The above contents are for plates of a single layer. To obtain the resonant frequency of plates made of multi-layers, one need to take the elastic potential energy and mass kinetic energy into consideration by modifying $k_{ij}$ and $m_{ij}$.

Assuming there is another layer of material on the top of the original plate. With the new layer added, there is a new flexural rigidity of the plate as a whole $D_t$ [51]. The additional layer has the young's modulus of $E_2$, the poison ratio of $\mu_2$, the thickness of $h_2$, and the density of $\rho_2$.

$$D_t = C - \frac{B^2}{A} \qquad \text{Equation 18}$$

, where

$$A = \frac{E_2 h_2}{1-\mu_2^2} + \frac{Eh}{1-\mu^2};$$

$$B = \frac{E_2\left((h+h_2)^2 - h^2\right)}{2\left(1-\mu_2^2\right)} + \frac{Eh^2}{2(1-\mu^2)};$$

$$C = \frac{E_2\left((h+h_2)^3-h^3\right)}{3\left(1-\mu_2^2\right)} + \frac{Eh^3}{3(1-\mu^2)}; \qquad \text{Equation 19}$$

Now, the new $k_{ij}$ and $m_{ij}$ can be written as:

$$k_{ij} = k_{ji} = \iint_s D_e \left\{(\nabla^2 \emptyset_i)(\nabla^2 \emptyset_j) - (1-\mu)\left(\frac{\partial^2 \emptyset_i}{\partial x^2}\frac{\partial^2 \emptyset_j}{\partial y^2} + \frac{\partial^2 \emptyset_i}{\partial y^2}\frac{\partial^2 \emptyset_j}{\partial x^2} - 2\frac{\partial^2 \emptyset_i}{\partial x \partial y}\frac{\partial^2 \emptyset_j}{\partial x \partial y}\right)\right\} dx\, dy$$

Equation 20

$$m_{ij} = m_{ji} = \iint_s \rho h \emptyset_i \emptyset_j \, dx\, dy + \iint_s \rho_2 h_2 \emptyset_i \emptyset_j \, dx\, dy \,, i, j = 1, 2, \cdots, n$$

Equation 21

Based on the identical boundary conditions in the previous cases, the fundamental angular frequency of a clamped rectangular plate with multi-layers is:

$$\omega = \frac{\sqrt{\frac{63}{2}\left(1+\frac{4a^2}{7b^2}+\frac{a^4}{b^4}\right)}}{a^2}\sqrt{\frac{D_t}{\rho h+\rho_2 h_2}} \qquad \text{Equation 22}$$

For the clamped square plate, Equation 20 becomes:

$$\omega = \frac{9}{a^2}\sqrt{\frac{D_t}{\rho h+\rho_2 h_2}} \qquad \text{Equation 23}$$

For the case of clamped circular plate, the corresponding fundamental angular frequency becomes:

$$\omega = \frac{10.21}{a^2}\sqrt{\frac{D_t}{\rho h+\rho_2 h_2}} \qquad \text{Equation 24}$$

Due to

$$f = \frac{\omega}{2\pi} \qquad \text{Equation 25}$$

The equations calculating resonance frequencies of a square plate and a circular plate with single layer are concluded separately as:

$$f_0 = \frac{9}{2\pi a^2}\sqrt{\frac{D}{\rho h}} \qquad \text{Equation 26}$$

, and

$$f_0 = \frac{10.21}{2\pi a^2}\sqrt{\frac{D}{\rho h}} \qquad \text{Equation 27}$$

The resonance frequency of four case studies calculated based on the vibration plate theory are concluded in Table 4-4.

Table 4-4 Resonance frequencies calculated from equations

| | Case study 1 | Case study 2 | Case study 3 | Case study 4 |
|---|---|---|---|---|
| $f_0$ | 608kHz | 3.14MHz | 4.64MHz | 5.61MHz |

### 4.2.2 Mass sensitivity

In terms of the frequency response of gas sensors based on the mass-loading effect, there is a main parameter: mass sensitivity. The mass sensitivity of a MEMS resonant sensor is defined as resonance frequency shift induced by the added mass attached to the sensor.

$$s_m = \frac{\Delta f}{\Delta m} \qquad \text{Equation 28}$$

According to the equation of calculating the mass ($m$) from the density ($\rho$) and the volume ($V$):

$$m = \rho \mathrm{V} \qquad \text{Equation 29}$$

Then, the resonance frequency is related to the mass of the plates.

For a square plate:

$$f_0 = \frac{9}{2\pi a}\sqrt{\frac{D}{m}} \qquad \text{Equation 30}$$

For a circular plate:

$$f_0 = \frac{0.83}{a}\sqrt{\frac{12D}{m}} \qquad \text{Equation 31}$$

Equation 30 and Equation 31 indicate that the resonance frequencies of a circular and a square plate are inversely proportional to the square roots of the mass of the resonant structures. Equation 32, the derivative of Equation 30 and Equation 31, illustrates that the amount of negative shift in resonance frequency, $df_0$, is directly proportional to the amount of loaded mass, $dm$.

$$df = -\frac{1}{2} \times \frac{f_0}{m} \times d\mathrm{m} \qquad \text{Equation 32}$$

## 4.3 Simulations

### 4.3.1 Introduction

Finite Element Methods (FEM) analysis is an effective analytical method for predicting the dynamic performance of PMUTs and CMUTs operating in conventional mode. ANSYS Multiphysics is the standard software for simulating MEMS devices. Recently, many institutions and researchers have started using COMSOL Multiphysics that is an alternative FEM simulation software with the rise in popularity. It is an incredibly powerful and useful tool, which can be used to solve a wide variety of engineering problem through its ability to couple built-in physics modules. Furthermore, COMSOL can simultaneously prove visual, graphical and numerical results, which offers a better learning experience for the users to allow them to grasp a firm understanding of their models.

In this section, the fist model of the PMUT and the second model of the 1st generation BCB CMUT are analyzed. The PMUT (case study 2) and CMUT (case study 3) are built in COMSOL Multiphysics (COMSL Co. Ltd) to simulate. The geometries are shown in Figure 4-8 and Figure 4-9 respectively. Due to rotation symmetry, the CMUT structure is built in 2D models, while the PMUT is built in 3D models. Because the PMUT cells are designed in squared-shape with simple structures, it is easier to model them in 3D instead of in 2D.

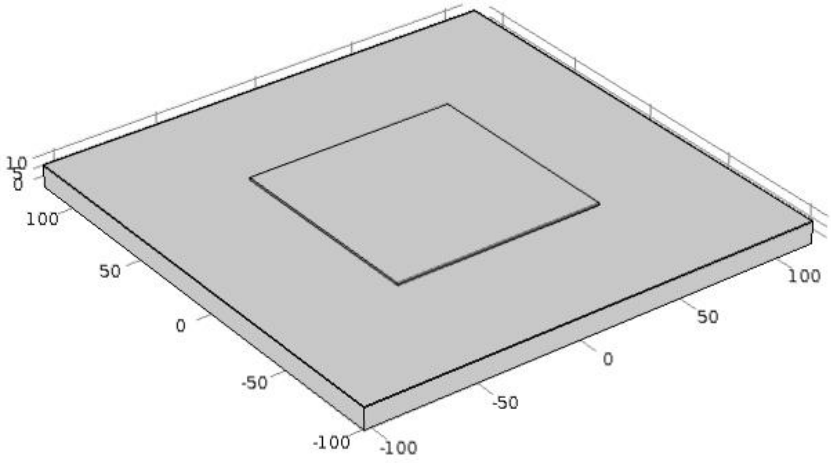


Figure 4-8 Geometry of the PMUT cell

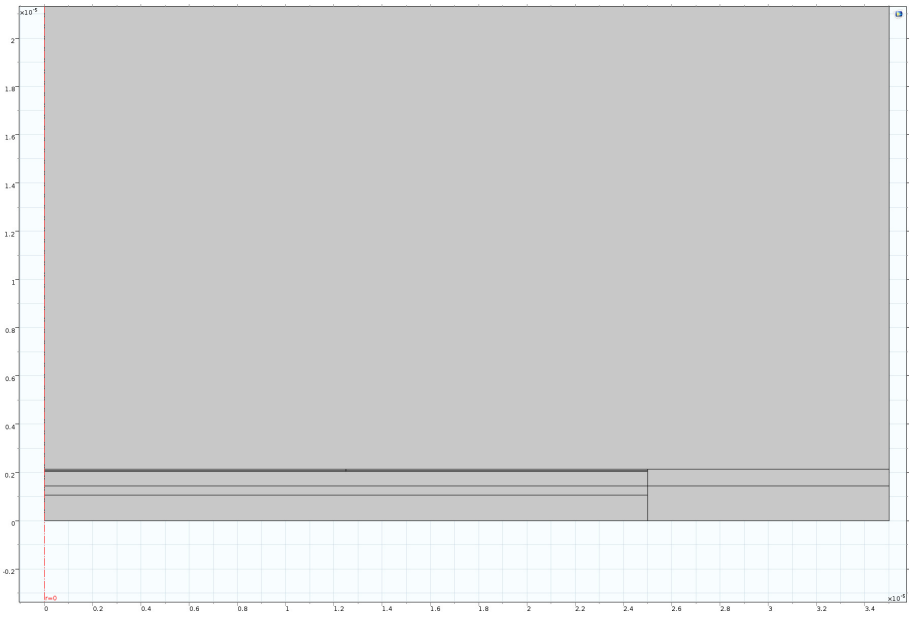

Figure 4-9 Geometry of the CMUT cell

### 4.3.2 Preliminary Setup

Before any analysis, the model is set up in COMSOL with the following steps (note: they may not be in the exact order):

1. 2D or 3D models are created following the specified structural dimensions listed before.
2. The materials used in transducers are defined under the Materials header. Then, the materials are applied to their respective components through domain selection.
3. The solid, electromechanics and acoustic pressure modules/ physics are then applied differently to the model. The boundary conditions are simultaneously initialized, such as linear Eleatic material, Ground, Terminal, and Fixed constraint.
4. The meshes applied to the structures are set up personally.
5. According to tasks for analysis, the studies are added to analyze.

### 4.3.3 Static Analysis

Both the PMUT and the CMUT are simulated firstly for static analysis. With the help of the FEA method, The PMUT models under air are discredited into thousands of triangle and tetrahedral meshes. The discretized meshes of PMUT models are shown in Figure 4-10.

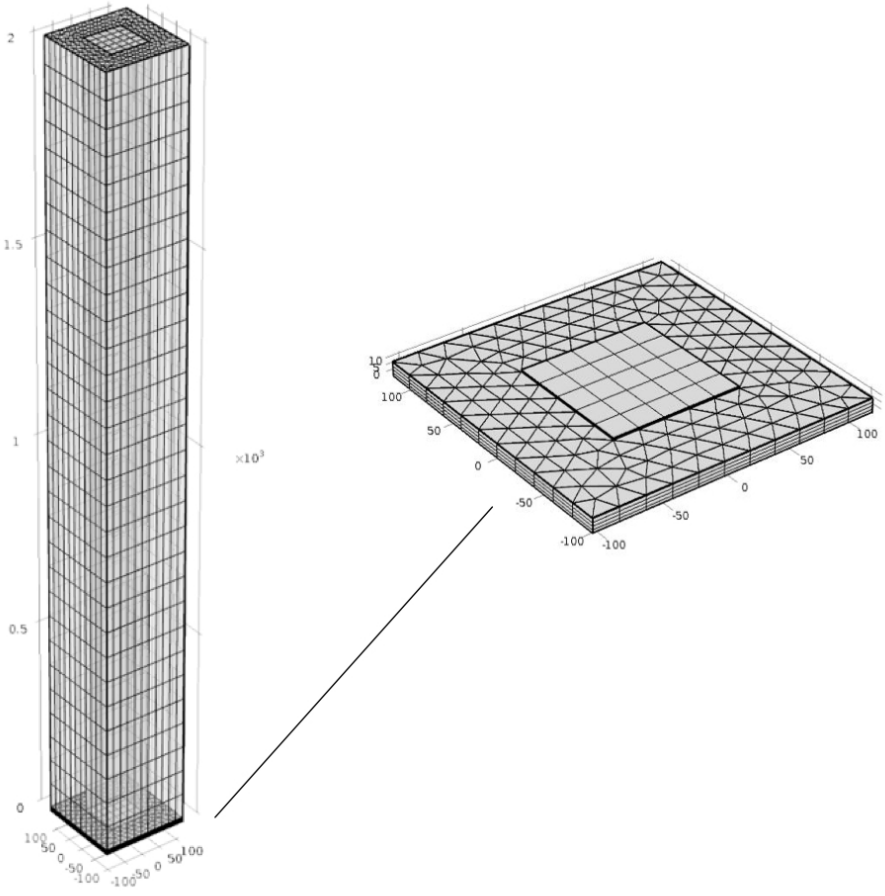


Figure 4-10 Meshing elements for the PMUT structure

For the CMUT simulation, the transducer is placed under air as well. The bias voltage applied to top electrodes are increased from 0V to pull-in voltage, and the bottom electrodes are kept at 0V. The target of this analysis is to estimate the pull-in voltage of the CMUT structure. When the membrane of the CMUT displaces from its equilibrium position by one-third, the electrostatic field dominates over structure stiffness and creates instability. As a result, the membrane is pulled towards to bottom electrode and contacts with it.

The meshes are built to get the desired responses. The tetrahedral mesh elements are shown in Figure 4-11, and the membrane displacement under DC (80V) is shown in Figure 4-12. The largest displacement is presented in the color of red, and the blue area illustrates a relatively small displacement. It can be found that the membrane attracts towards bottom electrode under the electrostatic force. The maximum displacement occurs at the center of the membrane. The direction of the excitation electric force is set along the direction of the Z axis, as such all modeled transducers

are pulled down, producing a concave shape. The Figure 4-13 presents the results of the static analysis of CMUTs, which are the center displacement versus the DC bias voltage curve. It is clear that the deflection due to the atmospheric pressure is 84.8nm with the remaining deflection due to the DC bias voltage. By varying the DC bias, the pull-in voltage calculated is 200V, and the dynamic analysis is performed at 80V.

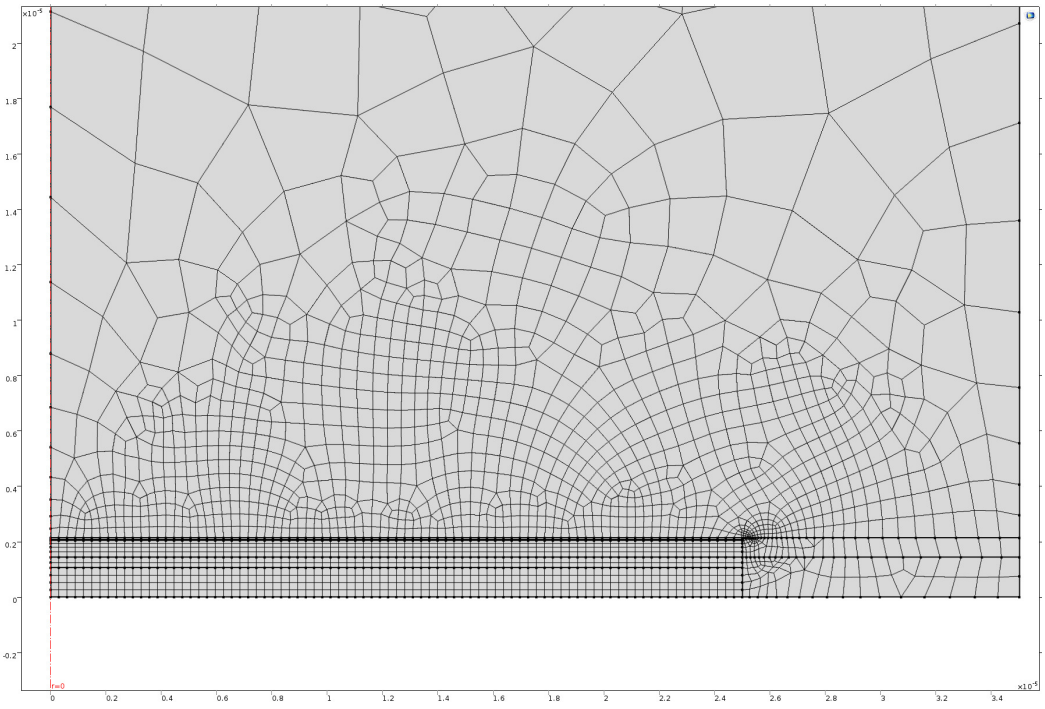

Figure 4-11 Meshing elements for the CMUT structure

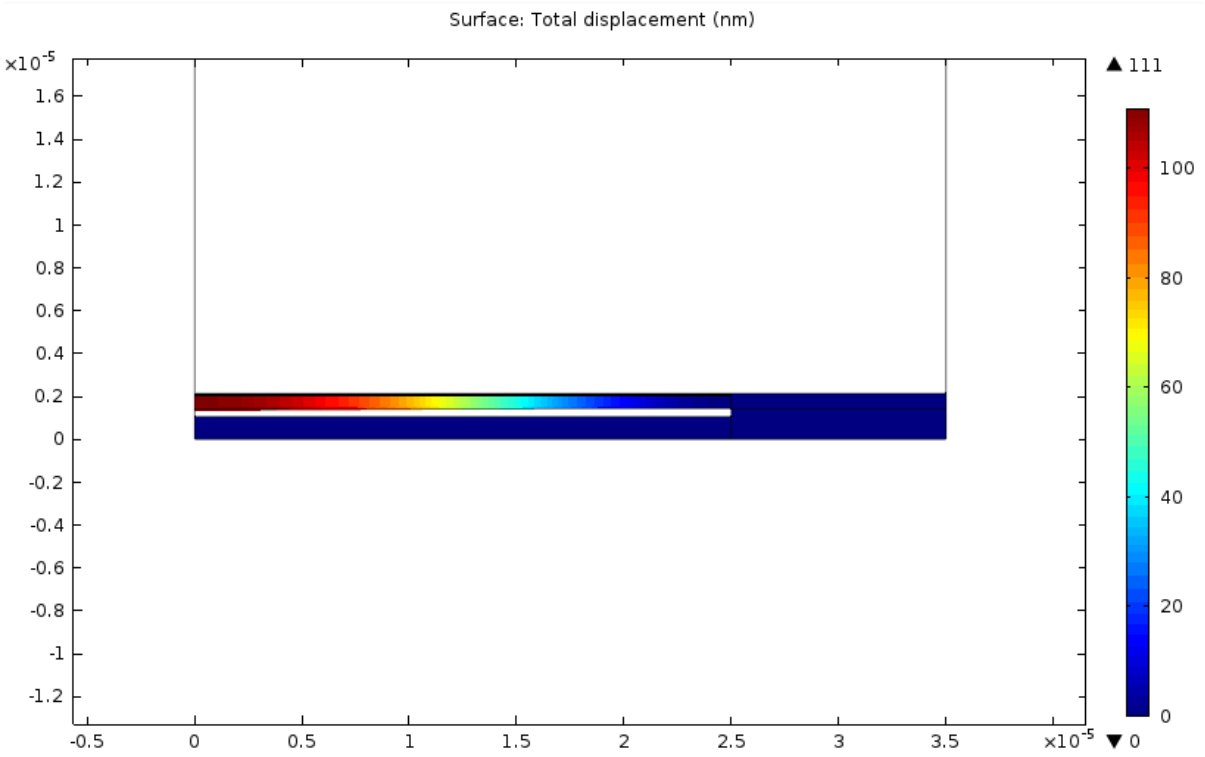


Figure 4-12 Displacement of the membrane when electric force (80V) is applied

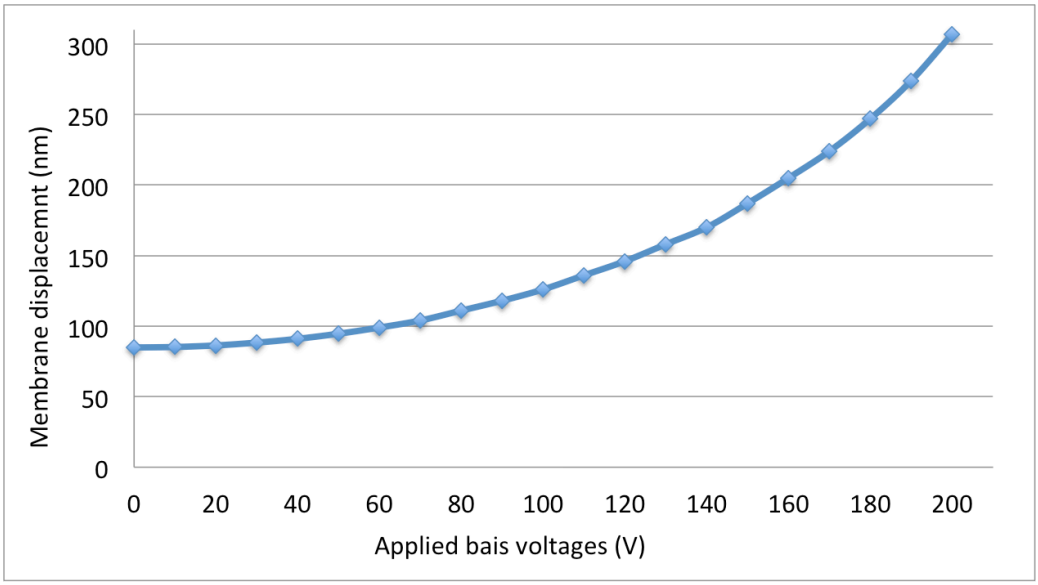


Figure 4-13 Center displacement of the CMUT as a function of pull-in voltage

### 4.3.4 Dynamic Analysis

In this section, the resonance frequency of the PMUT and CMUT can be estimated based on the magnitude of the displacement. For the PMUT, the frequency response of displacement amplitude under electrical excitation (1Vpp) is shown in Figure 4-14. The resonance frequency calculated is about 3.2MHz. The Figure 4-15 shows the shape of the PMUT at resonance frequency.

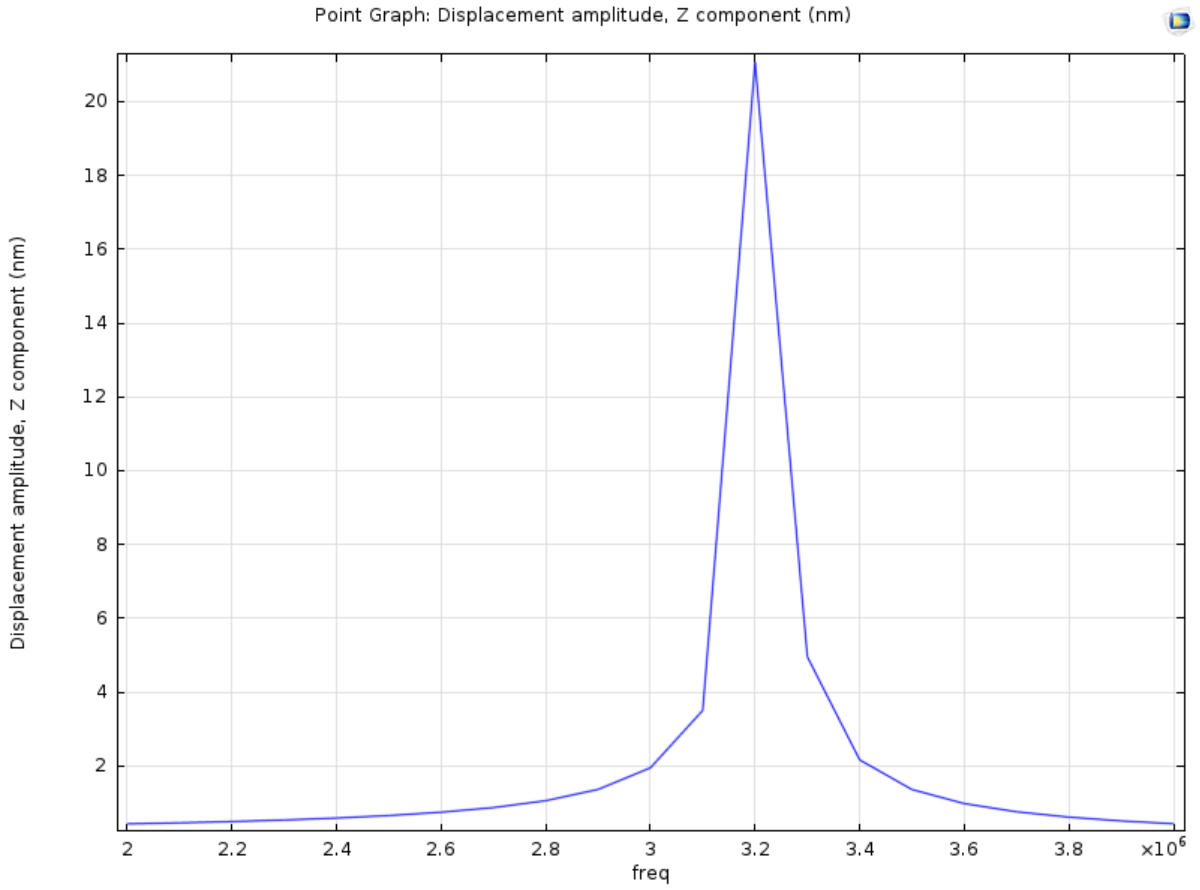


Figure 4-14 Frequency response of the center displacement of the PMUT

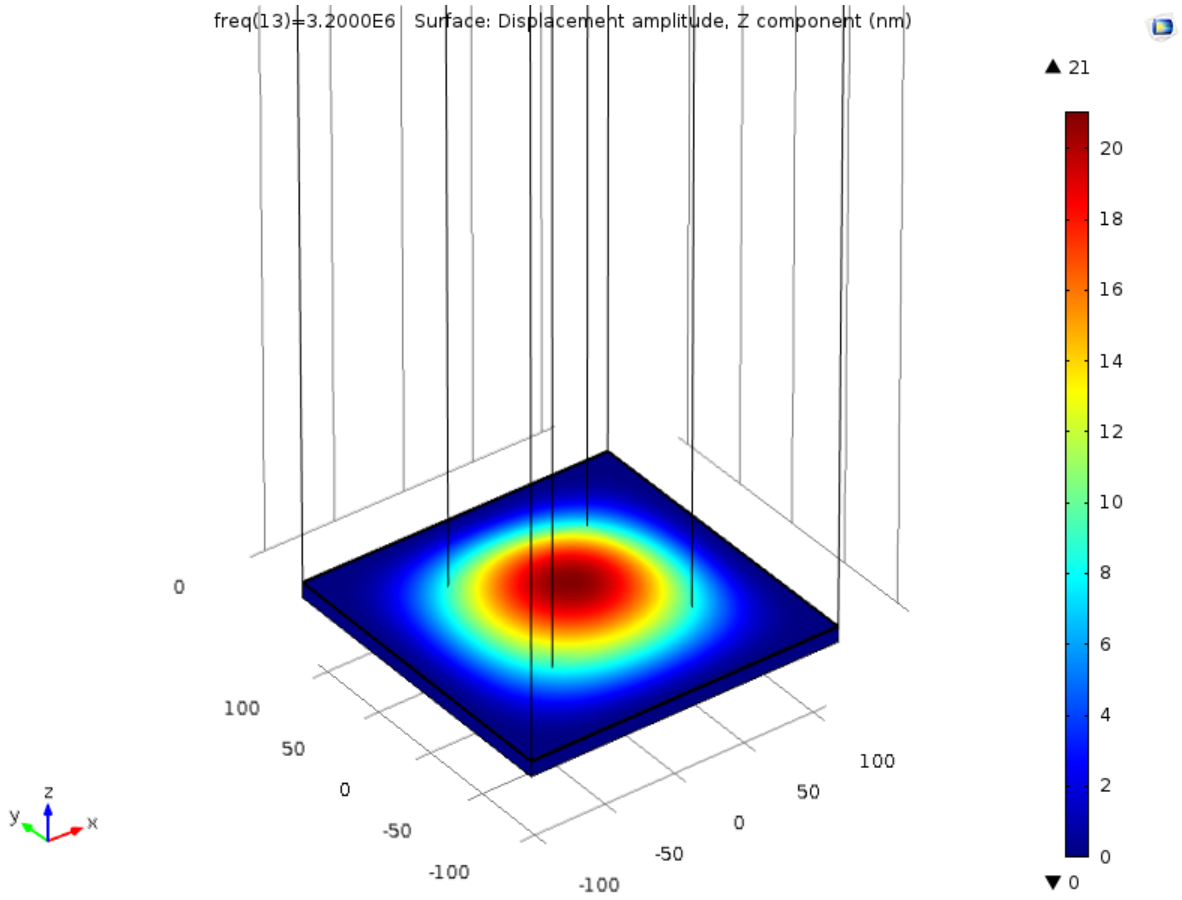


Figure 4-15 Displacement of the PMUT membrane at resonance frequency

The results represent the frequency response of the CMUT, as shown in Figure 4-16. Given the bias voltage, the models are excited by 1V AC voltage with several frequencies. Base on the results, the resonance frequency of the CMUT is 4.6MHz. The deformation of the CMUT at resonance frequency is shown in Figure 4-17. At the mean time, the resonance frequencies decrease with higher bias voltages due to the "spring softening effect" [52]. Additionally, as a result of the higher electric field through the gap, the amount of maximum displacement increases with the bias voltage.

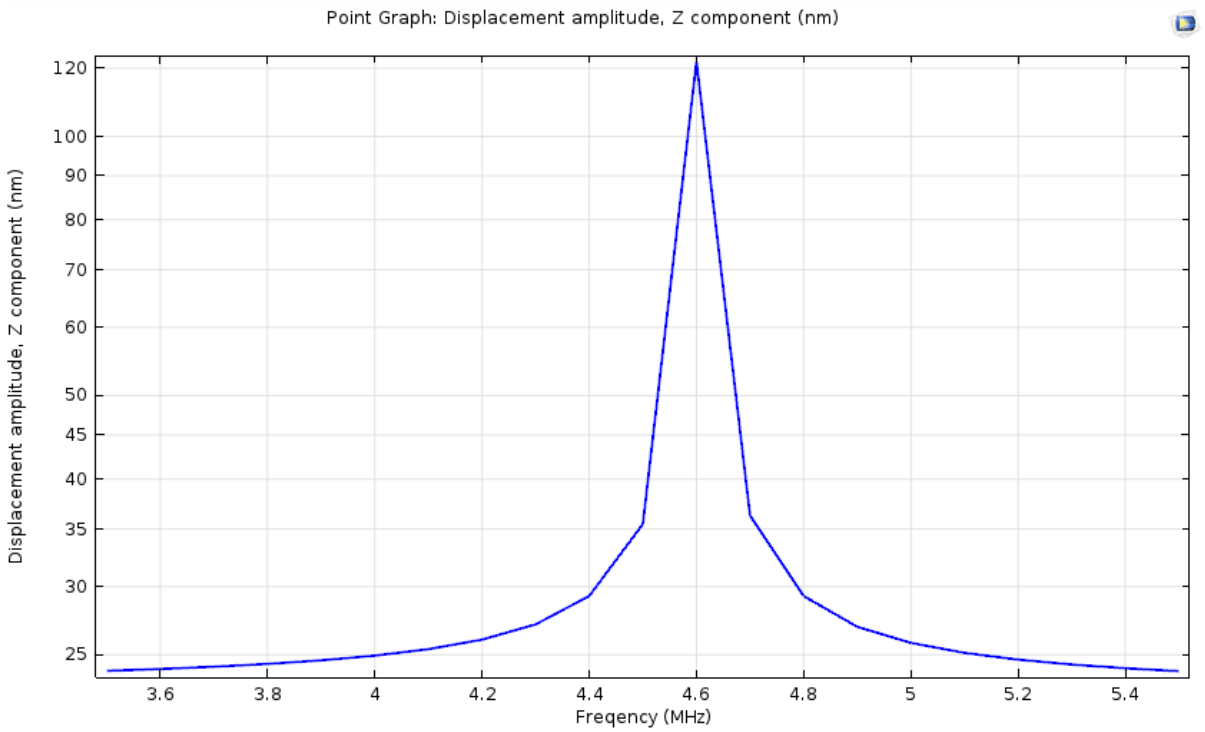


Figure 4-16 Frequency response of the center displacement of the CMUT

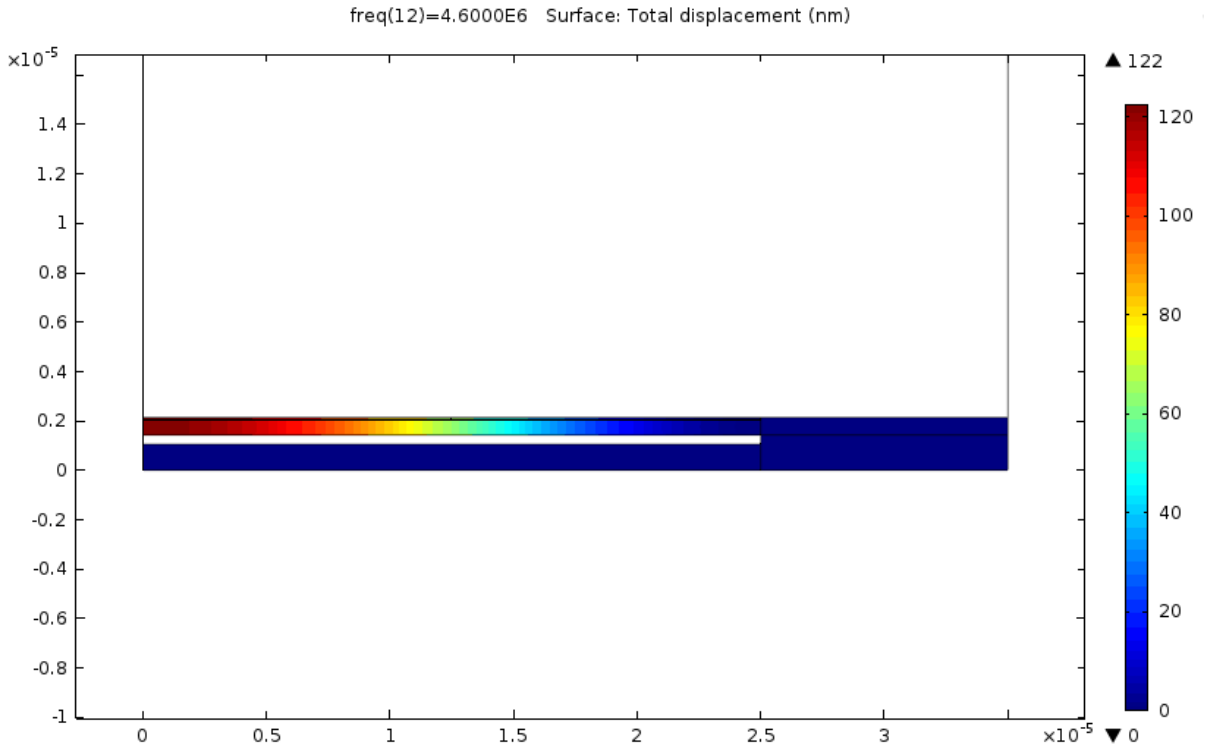


Figure 4-17 Displacement of the CMUT membrane at resonance frequency

### 4.3.5 Mass-loading Effect

To explain the principle of operation for gas sensing apparently, the mass-loading effect is considered in COMSOL as well. It is easier to use FEM rather than the analytic method because it requires fewer assumptions than the analytic method. Also, it is intuitively evident in FEM model to investigate the effect of the loaded mass on resonance frequency. The loaded mass applied on the plate can be defined by changing the density of the silicon plate [16]. For instance, if the loaded mass is 10% of the mass of the plate, the density of the plate in FEM is changed to 110% of its original density. In the simulations, the range of loaded mess is considered ranging from 10ppm to 10% of the plate's mess. The ppm stands for parts per million, which is a way of expressing very dilute concentrations of substances. Just as percent means out of a hundred, ppm refers to out of a million.

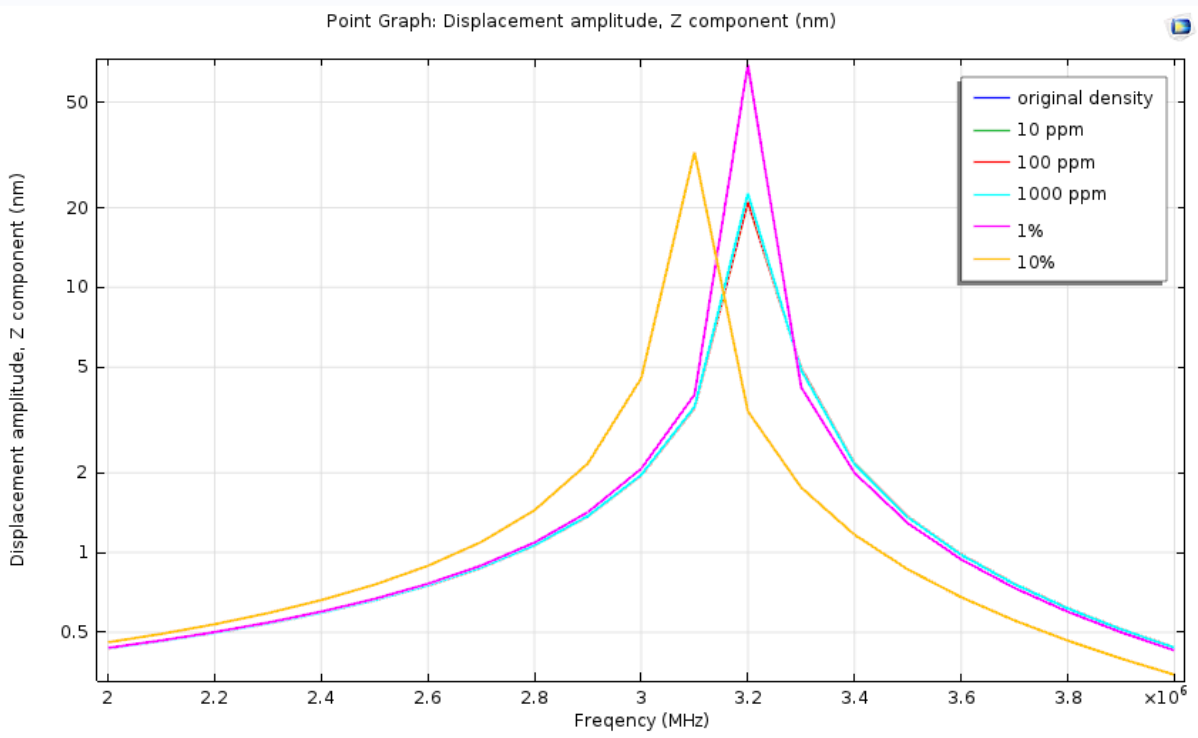


Figure 4-18 The effect of loaded mass on the resonance frequency of the PMUT

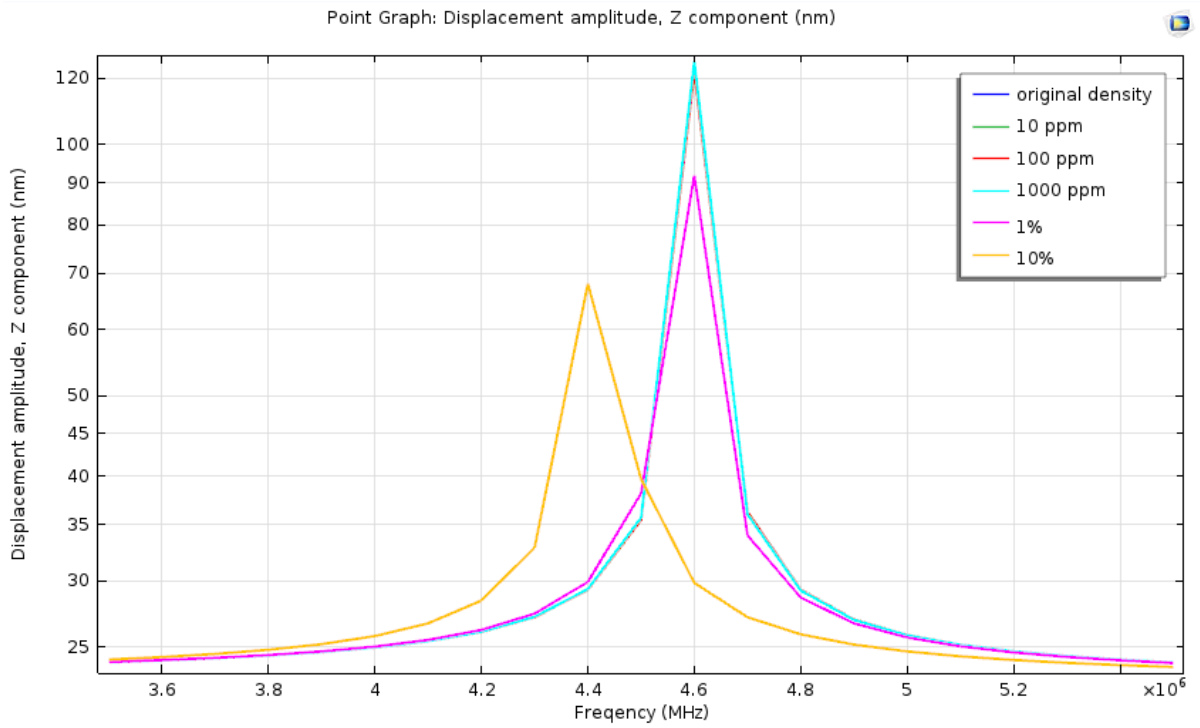


Figure 4-19 The effect of loaded mass on the resonance frequency of the CMUT

From the simulation results in COMSOL, as shown in Figure 4-18 and Figure 4-19, it is obvious that there is a negative frequency shift due to the increasing loaded mass. However, the frequency responses based on the results with a loaded mass ranging from 10ppm to 1% are similar. It is difficult to find the decrease of the resonance frequency when the density is increased by less than 1% because the changing of displacement is limited by the resolution of the frequency sweep and building mesh in the FEM modeling. To increase the frequency resolution, FEM requires more frequency points in the simulations. While, it is not practical to increase the frequency point to achieve 1Hz resolution in COMSOL simulations, which means the calculating process will go on infinitely.

## 4.4 Discussion

The devices of PMUTs and CMUTs used in this study are described firstly. The resonance frequency and mass sensitivity are analyzed by the analytic method based on the vibration plate theory. In the present works, the modeling and simulations are conducted in COMSOL Multiphysics FEM version

5.0, which includes the static analysis, dynamic analysis, and mass-loading effective analysis. The static analysis provides information about the transducer deflections under applied voltage change. The results of dynamic analysis of the PMUT and CMUT show the frequency response of displacement amplitude. Furthermore, according to the mass-loading effective simulations, the effect of loaded mass on resonance frequency is evident, which certifies that an increase in the mass of the resonant structure results in a decrease in the resonance frequency.

# Chapter 5
# Utilization of the PMUT and the CMUT for Ethanol Detection

## 5.1 Chemical Functionalization

To prepare the chemical experiment for ethanol detection, the PMUTs, and the CMUTs should be functionalized with thin sensing films firstly. The polymer has been widely applied in chemicals detection for resonant sensors, such as inorganic gas detection as well as VOCs or solvent vapors detection [53]. As mentioned before, when the polymer sensing films are exposed to the vapor of an analyte, the physical properties of the polymer such as mass and dielectric properties will change based on chemicals absorption. In this research, polyaniline (PANI) is chosen as sensing material. It can detect ethanol at room temperature or other low temperature [7]. Because of its porous structure, the ethanol molecule can be absorbed into the interstitial space of PANI, which causes its mass change.

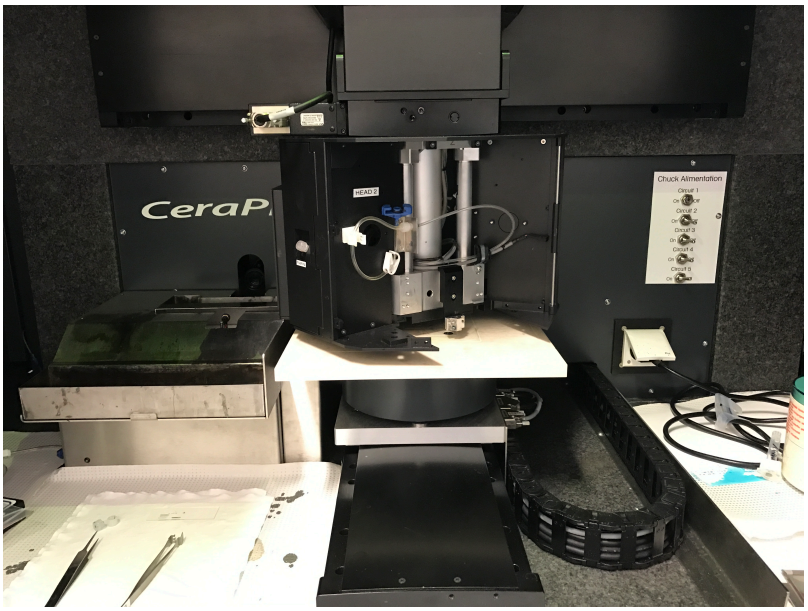


Figure 5-1 The Ceraprinter L-series system used for chemical functionalization

The PMUT and CMUT cells are deposited with a layer of PANI by using a multi-material inject printer (CeraPrinter L-series), as shown in Figure 5-1. It is a native multi-material inkjet printer, which ensures high process repeatability, high jetting accuracy, and broad materials compatibility. The principle of deposition is based on the drop-casting method under micron scale. The solution is dropped on a substrate, and the solvent evaporates spontaneously. A PANI solution is prepared before

deposition. 0.031g of PANI powder is added to 19.992g of N-Methyl-2-pyrrolidone (NMP) and then mixed using a sonicator for 30 minutes at room temperature. During the chemical functionalized process, the 0.15% PANI with NMP solution is filtered by a 1μm filter then installed to the printer. Around 50pL of each droplet of PANI dispersion controlled by the system are ejected from the equipment on the transducers.

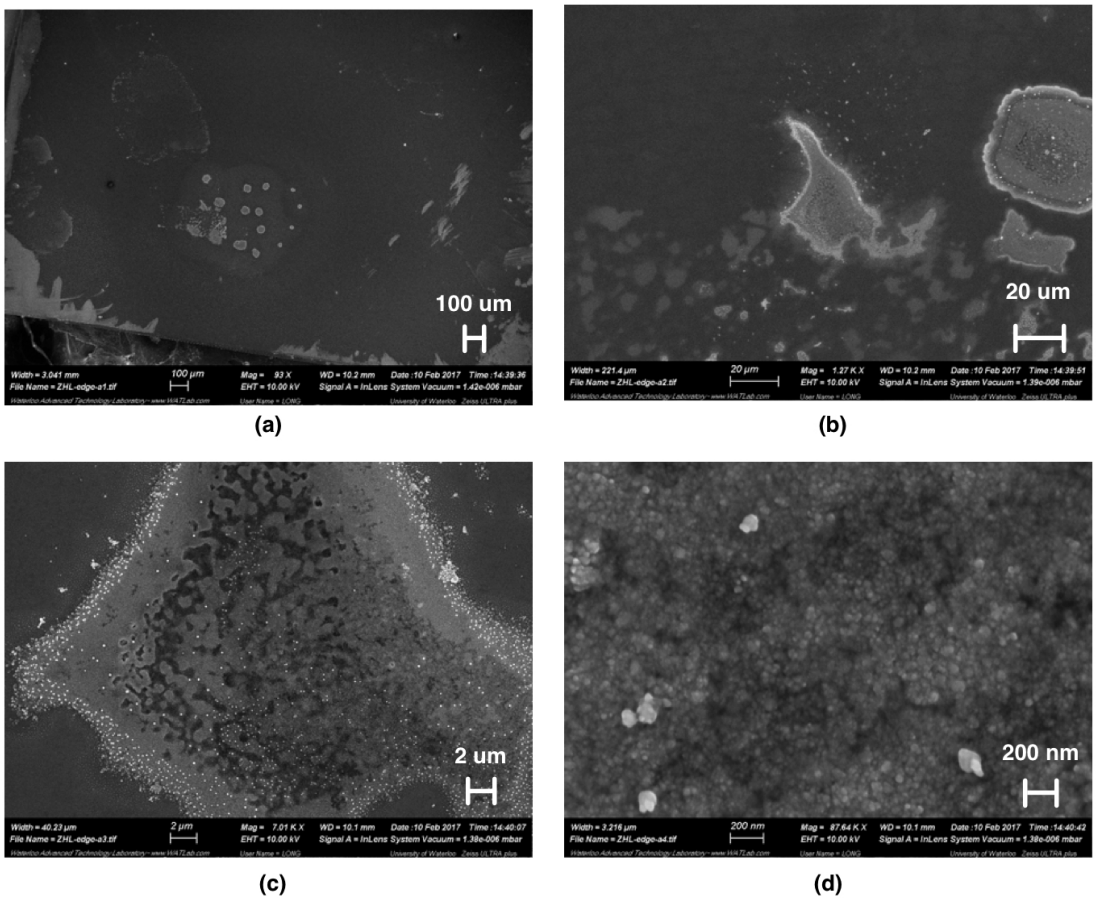


Figure 5-2 SEM images for 0.15% PANI deposited with one droplet a) under 100 μ m, b) under 20 μ m, c) under 2 μ m, d) under 200nm

The PANI films deposited by the micro printer are characterized under the scanning electron microscope (SEM). The Figure 5-2 shows the SEM images of PANI ejected with only one droplet on silicon wafer: a) is under 100μm resolution, b) is under 20mm, c) is under 2mm, and d) is under 200nm. The gray color represents the PANI particles. The diameters of PANI films are around

100mm. Based on the Figure 5-2 (d), it can be found that the single PANI particle is close to each other, and some particles are overlapped.

Then, by increasing the times of ejection to 10 (each ejection includes one droplet), the PANI film with the diameter about 500μm is shown in Figure 5-3 under the different resolution. Due to the surface tension, the PANI particles at the center of the film are diluted. So, the dispersion of the PANI particles is more uniform.

In the chemical experiment, to improve the performance of sensing film, it can be achieved by either increasing the concentration of PANI solution or repeating the deposition process. The concentration of PANI solution is increased to 0.2%.

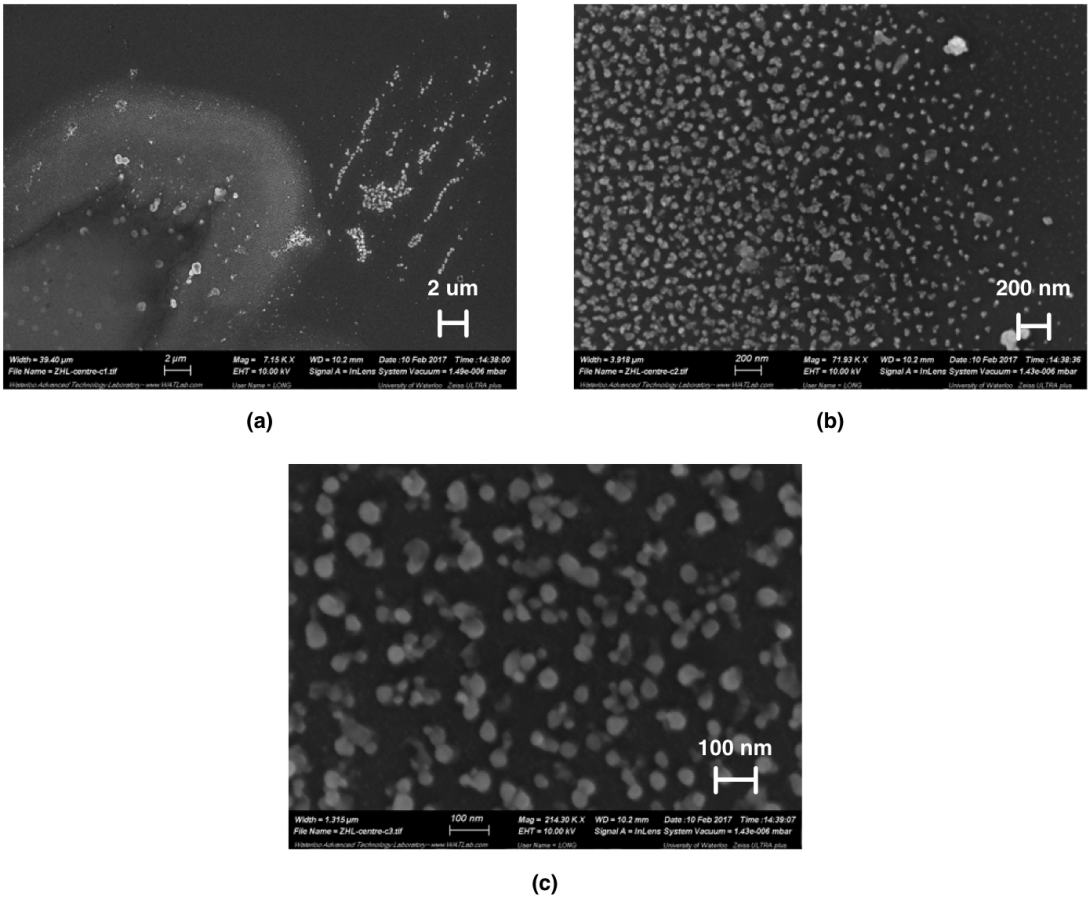


Figure 5-3 SEM images for 0.15% PANI deposited with 10 droplets a) under 2 μ m, b) under 200nm, c) under 100nm

## 5.2 Chemical Experiment

A typical Laser Doppler Velocimetry (LDV) experimental setup, as shown in Figure 5-4, makes it possible to investigate the effect of the mass change caused by gas molecule on resonance frequency through a single sensing element of transducers. The Laser–Doppler vibrometer (Polytec OFV-5000) is used in the experiments to measure out-of-plate displacements of vibrating surfaces in the nanometer range. The laser beam from the LDV is directed at the membrane of PMUTs or CMUTs, and the vibration amplitude and frequency are extracted from the Doppler shift of the reflected laser beam frequency due to the motion of the membrane.

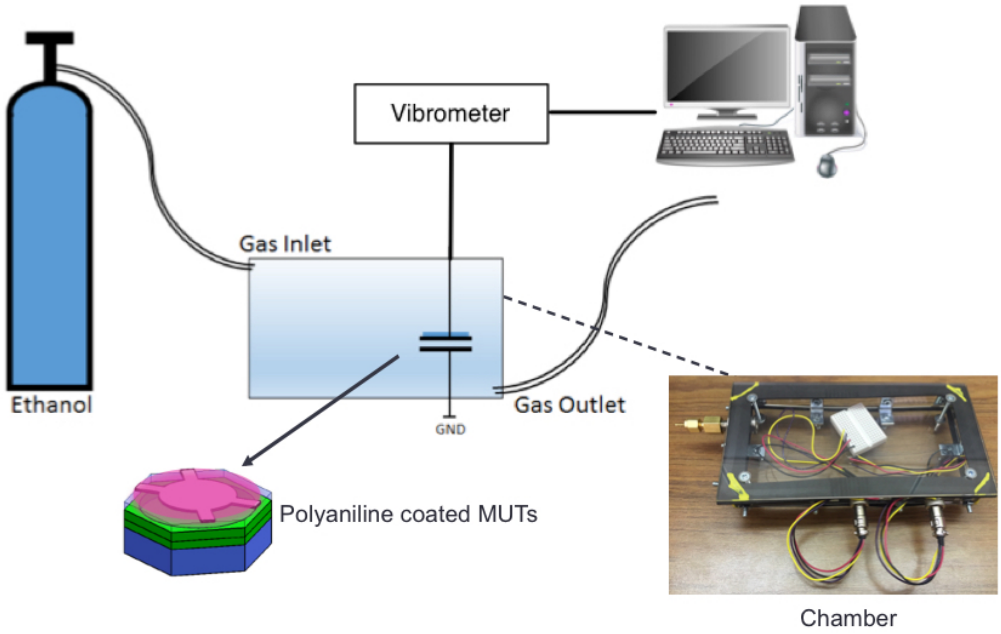


Figure 5-4 Experiment set up for ethanol detection

The PMUTs and CMUTs are placed dividedly in the chamber fixed on the mobile platform. For PMUTs actuation, a 20V peak-to-peak continuous-wave sinusoidal signal is applied across the electrodes using a function generator ((Tektronix AFG3022B). While for CMUTs actuation, an AC driving voltage, superimposed on a DC bias voltage, is added to CMUTs. Both the vibrometer and the function generator are connected to an oscilloscope for multipoint scanning. By sweeping the frequency signal, the displacement becomes maximum is defined as the resonant frequency of displacement response. This is a simpler approach to prove the feasibility of fabricated CMUTs and PMUTs for gas sensing.

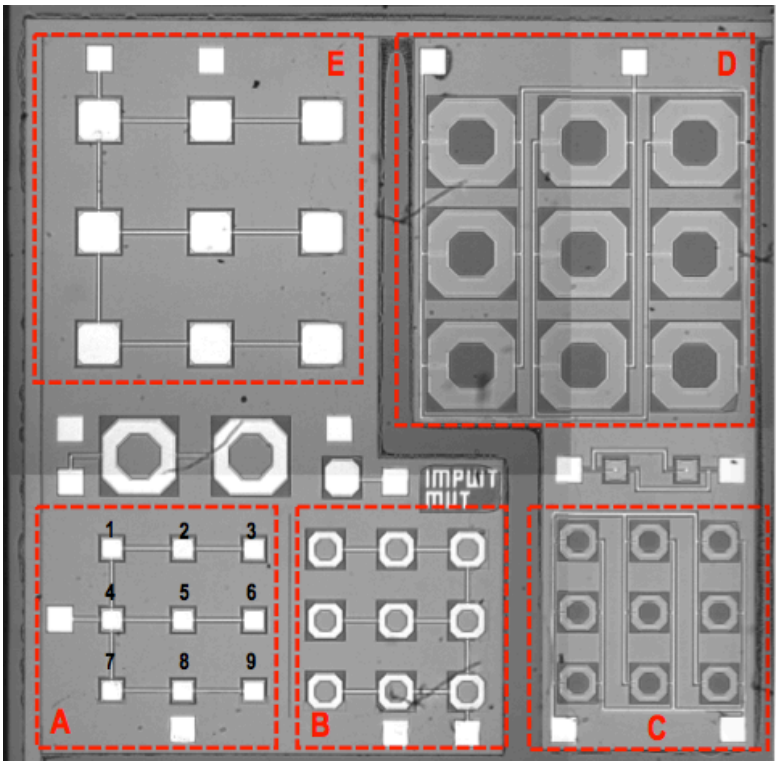


Figure 5-5 An Overview of PMUTs.

As shown in Figure 5-5, there are five PMUT elements on a chip. A, B and C are for higher frequency while D and E are for lower frequency. Each PMUT element consists of 9 cells in a three by three configuration labeled from 1 to 9. In the first experiment of ethanol detection using PMUTs, elements E (case study 1) and A (case study 2) are used for gas sensing. Cells 1 to 4 of each element are functionalized with PANI films, while others are used as references. The results are shown in Table 5-1 and Table 5-2. The frequency responses of single PMUT cell are measured under the concentration of ethanol at 100g/L. In the case study 1, the resonance frequency of E measured in air is 600kHz, and the frequency shift is around 1kHZ after ethanol ejecting to the chamber. In the case study 2, the resonance frequency of A measured is 2.3MHz, and the frequency shift is around 5kHz. The PMUT cell vibration shape scanned by vibrometer multi-point scanning is shown in Figure 5-6.

The results verify the effect of loaded mass on the resonance frequency of PMUTs. Furthermore, it is clear that the higher resonance frequency of PMUTs results in a higher frequency shift corresponding to the gas analyte, which means that the higher resonance frequency of transducers, the higher sensitivity of gas sensors.

Table 5-1 Case study 1 frequency response of a PMUT cell to 100g/L ethanol

| | E1 | E2 | E3 | E4 |
|---|---|---|---|---|
| No film (kHz) | 600 | 600 | 600 | 600 |
| PANI (kHz) | 570 | 572 | 578 | 578 |
| PANI + ethanol (kHz) | 569 | 571.6 | 576.8 | 576.6 |
| Frequency shift (kHz) | 1 | 0.4 | 1.2 | 1.4 |

Table 5-2 Case study 2 frequency response of a PMUT cell to 100g/L ethanol

| | A1 | A2 | A3 | A4 |
|---|---|---|---|---|
| No film (MHz) | 2.3 | 2.3 | 2.3 | 2.3 |
| PANI (MHz) | 2.114 | 2.131 | 2.153 | 2.121 |
| PANI + ethanol (MHz) | 2.108 | 2.128 | 2.15 | 2.114 |
| Frequency shift (kHz) | 6 | 3 | 3 | 7 |

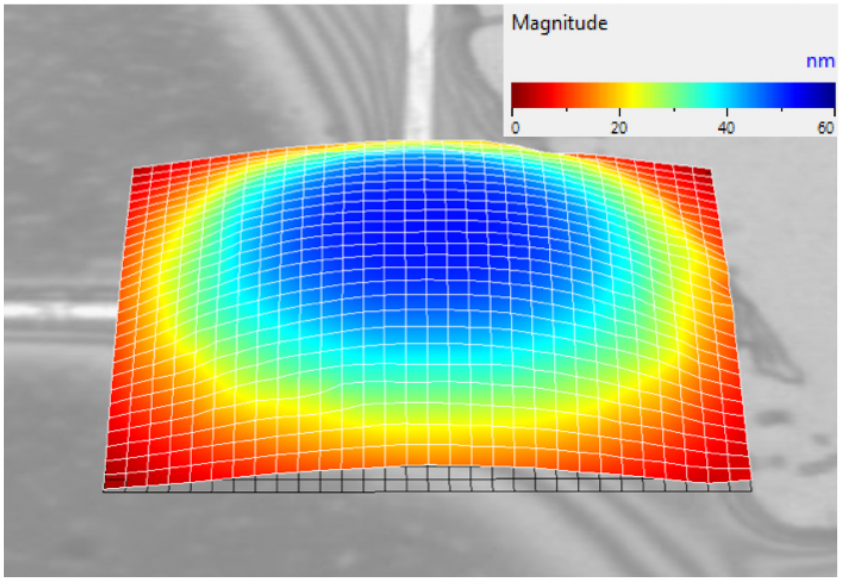


Figure 5-6 Vibrometer multi-point scan showing the PMUT cell vibration shape

According to the results of frequency shift on PMUTs in ethanol detection experiments, the experiment of ethanol detection using CMUTs is based on the CMUTs with higher resonance

frequency at 6.4MHz measured by vibrometer (case study 4). Due to the fabrication process, the thickness distribution of Silicon Nitride deposited over entire wafer is various [32]. Therefore, the CMUT with a thicker SiN membrane shows a higher resonance frequency. The results of the frequency response of a single CMUTs cell corresponding to ethanol are shown in Figure 5-7 and Figure 5-8. The cell for measuring is selected randomly. The frequency responses of CMUT cell are measured firstly under the concentration of ethanol at 100g/l as well. The resonance frequency shift of the single CMUT cell is around 50kHz corresponding to ethanol. Then, the concentration of ethanol is decreased to 1000ppm. One ppm is equivalent to 1 milligram of something per liter (mg/l), so 1000ppm is $10^{-2}$ times of 100g/l. The frequency shift of the single CMUT cell is around 14kHz. The vibrometer multi-point scan evaluates the CMUT cell vibration shape, as shown in Figure 5-9.

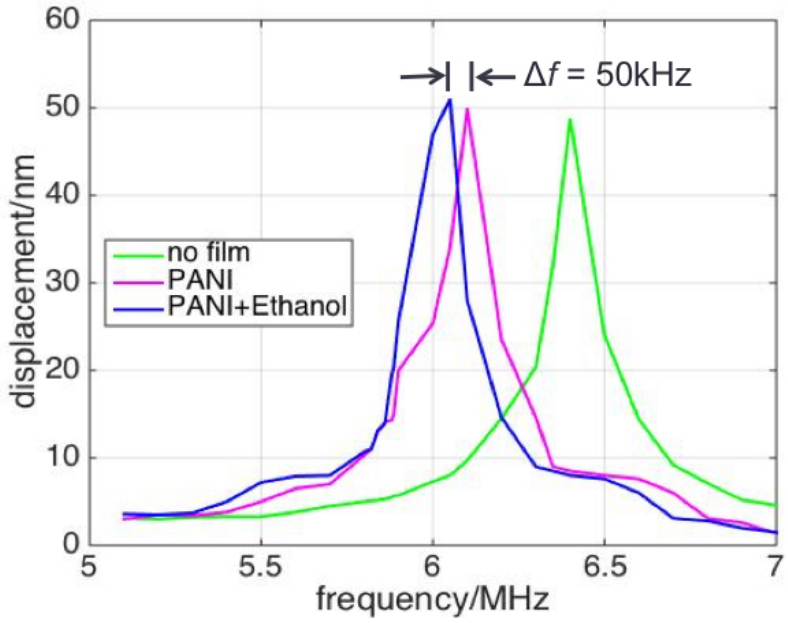


Figure 5-7 Case study 4 frequency response of a CMUT cell to 100g/L ethanol

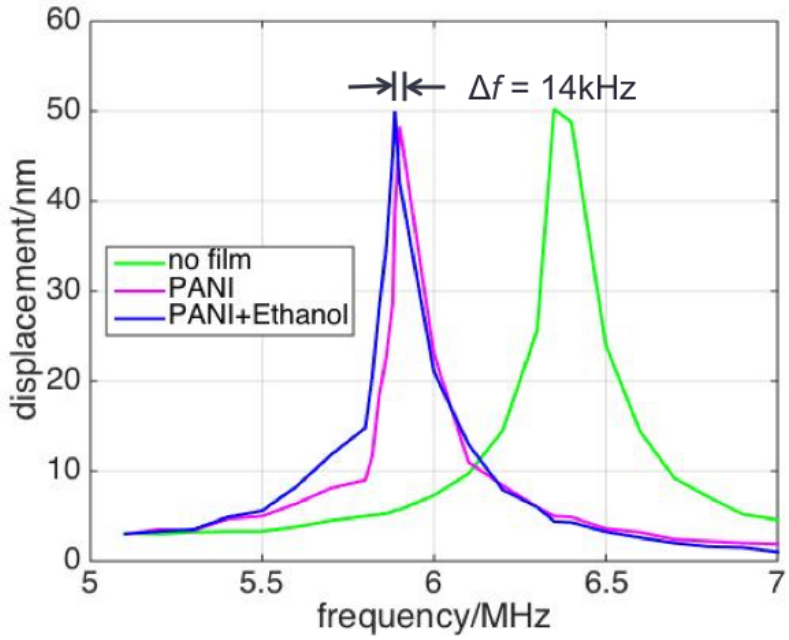


Figure 5-8 Case study 4 frequency response of a CMUT cell to 100g/L ethanol

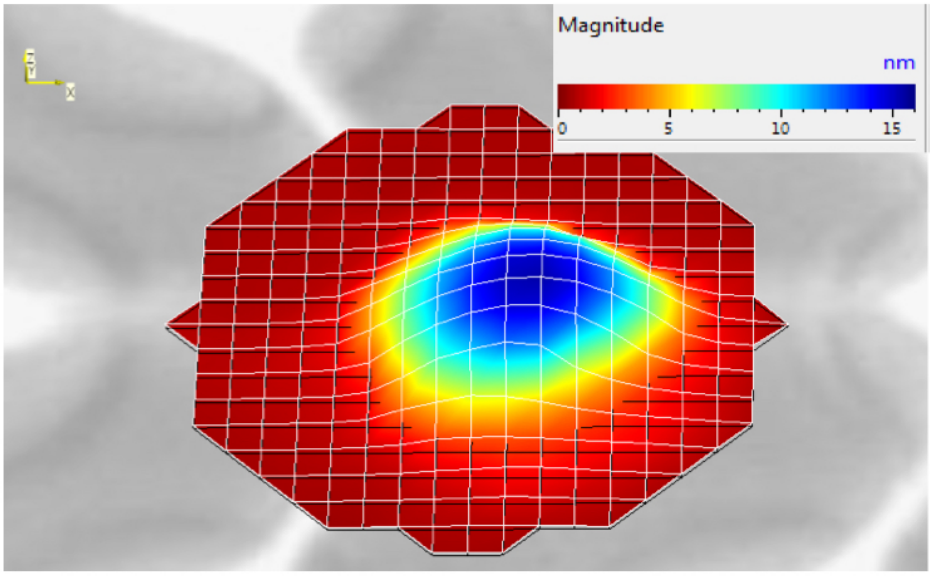


Figure 5-9 Vibrometer multi-point scan showing the CMUT cell vibration shape

Moreover, because CMUTs are easily fabricated in an array, the experiment of ethanol detection by measuring the frequency response of a CMUT array is also investigated in this thesis. The experiment set is shown in Figure 5-10. The 2nd generation CMUT in an array including 3520 cells is

used. The network analyzer (Rohde & Schwarz ZNB 20) takes the place of the vibrometer in this part. The vibrometer focuses on a single cell for frequency response measurement by directly testing the displacement of a resonant structure, while the network analyzer can evaluate the resonance effect of entire CMUT element by measuring the impedance of CMUT. The magnitude of the impedance is plotted in Figure 5-11. The resonance frequency of CMUT array is about 5.4MHz, and the frequency shift of resonance is around 10kHz under 1000ppm ethanol. The Figure 5-12 shows the CMUT array vibration shape.

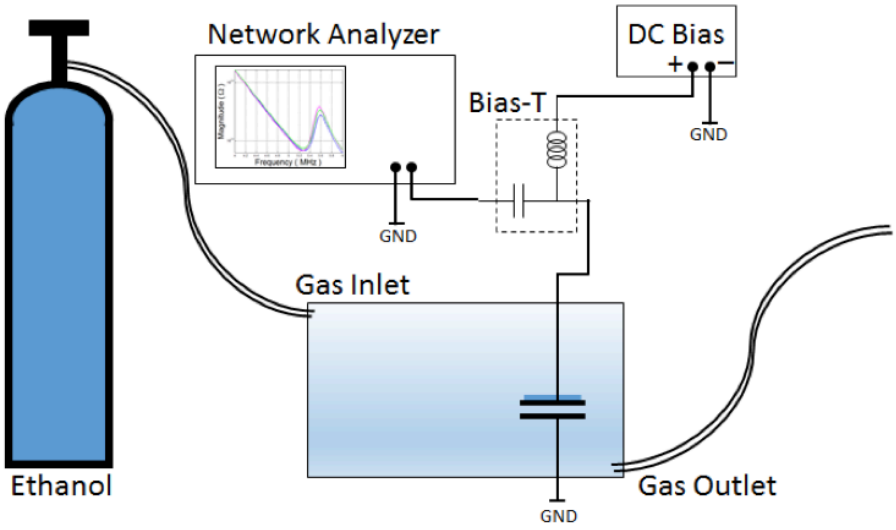


Figure 5-10 Experiment set up for ethanol detection using CMUT array

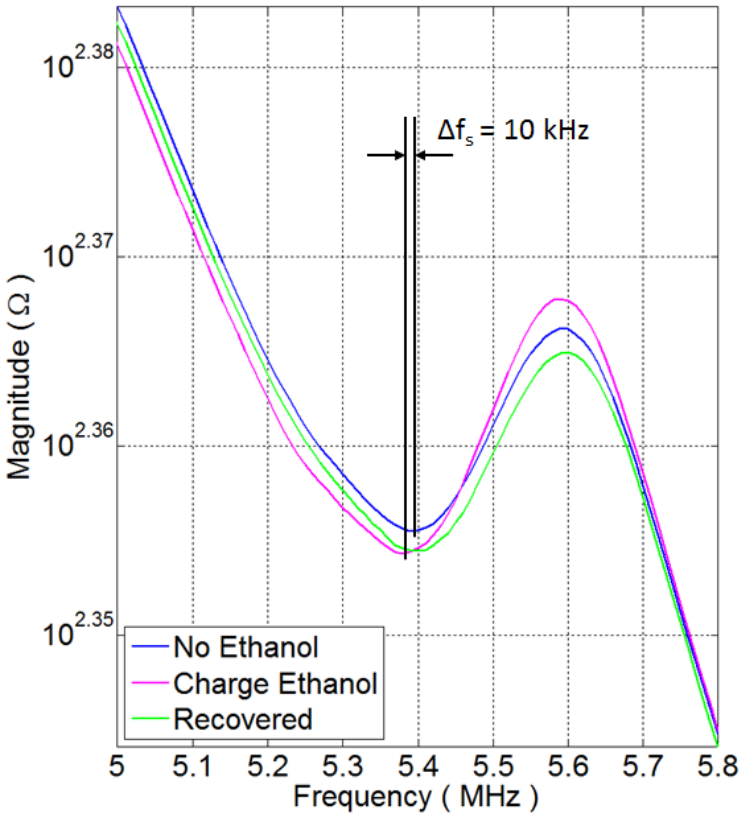


Figure 5-11 Case study 3 frequency response of a CMUT array to 1000ppm ethanol

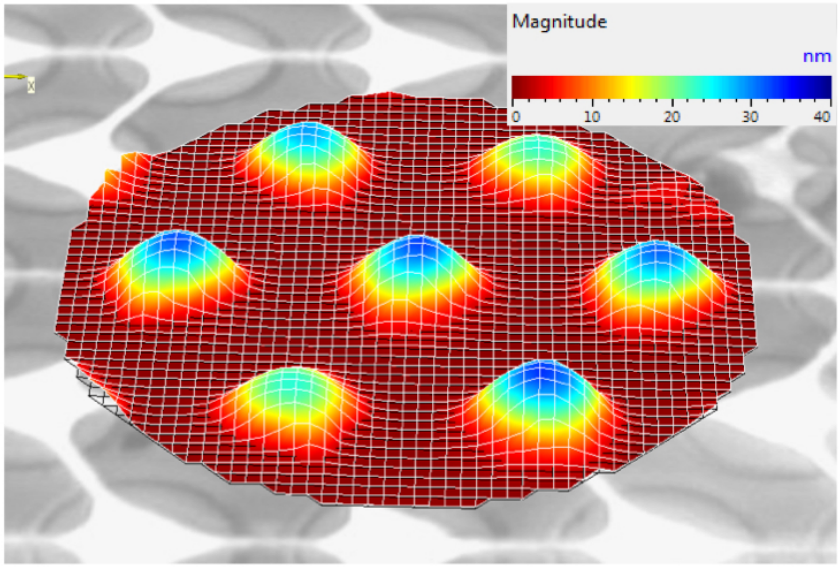


Figure 5-12 Vibrometer multi-point scan showing the CMUT array vibration shape

## 5.3 Discussion

This chapter demonstrates a primary feasibility study of PMUTs and CMUTs for ethanol detection. After the simulations, the chemical functionalization and chemical experiment are presented in this chapter. The results confirm that the effect of loaded mass on resonance frequency, which proves that the PMUTs and CMUTs fabricated by our lab can be applied to multiple applications.

In the PMUTs experiment, for PMUTs' resonance frequency at 600kHz and 2.3Mhz, the frequency shifts measured are 1kHz and 5kHz respectively under 100g/l ethanol gas phase. It is clear that the resonance frequency is related to the sensitivity. In the CMUTs experiment, the CMUT's resonance frequency at 6.4MHz is used to get higher sensitivity. Under the concentration of ethanol at 100g/l, the frequency shift is 50kHz, and under the concentration of ethanol at 1000ppm, the frequency shift is 14kHz. It illustrates that the lower concentration of ethanol can be detected, when resonance frequency of transducer is increased. Moreover, the $2^{nd}$ generation CMUT in array is used in ethanol detection as well. The resonance frequency of CMUT array is measured at 5.4MHz. Due to the fabrication process of deposition SiN membrane, the thickness of the SiN layer varies, which results in the lower resonance frequency of CMUT (in array) placed at the edge of wafer [32]. The frequency shift is about 10kHz under 1000ppm ethanol. It also provides a potential of using CMUTs array functionalized with different sensing material for chemical detection in future.

# Chapter 6
# Conclusion

## 6.1 Summary

This thesis illustrates a feasibility study of using the fabricated CMUTs and PMUTs for ethanol detection. It provides a simple method to investigate the effect of loaded mass on resonance frequency directly by the frequency shift measurement. However, in practice, it is impossible to measure the frequency shift using the vibrometer. The CMUTs and PMUTs are desired to be integrated with oscillators, which can convert the frequency shift to the electric signals corresponding to the gas information. According to the flip-chip bonding or wire bonding technique, CMUTs and PMUTs have superior abilities to be integrated with supporting electronics, which can reduce the cost and increase the portability of the devices for gas sensing [54][55]. More importantly, by applying the flip-chip bonding technique, transducers and electronic circuits can be designed and manufactured separately providing high design flexibility.

It is hard to summarize that whether CMUTs have better performance than PMUTs for gas sensing. They can be compared with the following items, which can provide some instructions for future studies for researchers. First of all, sensitivity is the biggest difference between PMUTs and CMUTs. CMUT membranes can be pulled down with a biased voltage. The pull-down action results in the spring softening effect, which could theoretically achieve high sensitivity (and in practice still quite high compared to PMUTs) [56]. PMUTs do not have that luxury.

The fill-factor is another considerable aspect. Because of the way that PMUTs are fabricated (through-wafer etching from the bottom), it results in a low fill-factor [57][58]. In another word, it can put more CMUTs than PMUTs in the same area.

Additionally, MEMS fabrication techniques that are required for achieving CMUT structure enable the batch production of high-frequency ultrasonic transducers in the form of arrays with small feature size (sub-micron level).

However, the operating voltage of CMUTs is extremely high, e.g., over 100 V. Such high voltage generates safety concerns and limits possible applications of CMUT. As an alternative, PMUTs is driven using piezoelectric effect, which enables PMUTs to operate at a much lower voltage in comparison to CMUTs [59]. It is easy to construct an oscillator for PMUTs. Since a high bias

voltage is not desirable in the low power circuits, PMUTs do have an advantage from circuit implementation's perspective.

At present, PMUTs is still in a very early stage of development. Comparing to the conventional ultrasound transducers and CMUTs, only a relatively limited number of publications on PMUTs has appeared over the last 25 years. It may be attributed to two reasons: the difficulties in the manufacture of high performance piezoelectric thin films, and the lack of efficient modeling methods or tools for accurate prediction of the effects of intrinsic stress. These challenges have therefore led to developing PMUTs with lower performance in practice than theory [55].

## 6.2 Future Direction

There are two potentials for improving the current experiments concerning a very sensitive MUT-based chemical sensor.

- Improving the resonance frequency of PMUTs or CMUTs by optimizing structural dimensions. The current PMUTs and CMUTs are designed and fabricated for medical applications, which may not be compatible with the required design as gas sensors.
- Optimizing the chemical functionalization. It includes improving the concentration of PANI in sensing layer and controlling the thickness of sensing film. Due to the solubility of PANI in the organic solution is relatively low, which influences the concentration of PANI in sensing layer and sensitivity of gas sensors. Therefore, the PANI with higher solubility should be devised to realize a better gas sensor design. Furthermore, although a thicker sensing layer might be able to absorb more analyte in the carrier gas, according to previous studies it may result in some side-effects, such as increasing the time constant of absorbing molecules [16]. So for the chemical functionalization, the thickness of sensing layer should be investigated at a trade-off point.

# Bibliography


[1] Solomon, R., et al. "The 2012 Provincial and Territorial Legislative Review." *Oakville, ON: MADD Canada* (2012).

[2] Sullivan, Andrew. "Ending Drunk Driving with a Flash of Light." *Rich. JL & Tech.* 21 (2014): 1.

[3] Webster, Gregory D., and Hampton C. Gabler. "Feasibility of transdermal ethanol sensing for the detection of intoxicated drivers." *Annual Proceedings/Association for the Advancement of Automotive Medicine*. Vol. 51. Association for the Advancement of Automotive Medicine, 2007.

[4] Chen, Wei-Ting Scott, et al. "Wearable RF Sensor Array Implementing Coupling-Matrix Readout Extraction Technique." *IEEE Transactions on Microwave Theory and Techniques* 63.12 (2015): 4157-4168.

[5] Kupari, Markku, et al. "Breath acetone in congestive heart failure." *The American journal of cardiology* 76.14 (1995): 1076-1078.

[6] González-Chavarri, J., et al. "ZnO conductometric sensor for indoor air quality measurement inside buildings." *Electron Devices (CDE), 2015 10th Spanish Conference on*. IEEE, 2015.

[7] Winther-Jensen, Orawan, Robert Kerr, and Bjorn Winther-Jensen. "Alcohol vapour detection at the three phase interface using enzyme-conducting polymer composites." *Biosensors and Bioelectronics* 52 (2014): 143-146.

[8] Stewart, Katherine Mariann Elizabeth. "Design of Polymeric Sensing Materials for Volatile Organic Compounds: Optimized Material Selection for Ethanol with Mechanistic Explanations." (2016).

[9] Liu, Xiao, et al. "A survey on gas sensing technology." *Sensors* 12.7 (2012): 9635-9665.

[10] Yamazoe, Noboru, and Kengo Shimanoe. "Theory of power laws for semiconductor gas sensors." *Sensors and Actuators B: Chemical* 128.2 (2008): 566-573.

[11] Niskanen, Antti J., et al. "Atomic layer deposition of tin dioxide sensing film in microhotplate gas sensors." *Sensors and Actuators B: Chemical* 148.1 (2010): 227-232.

[12] Wang, Yun, and John TW Yeow. "A review of carbon nanotubes-based gas sensors." *Journal of Sensors* 2009 (2009).

[13] Lee, Hyunjoo J., et al. "Functionalization layers for CO 2 sensing using capacitive micromachined ultrasonic transducers." *Sensors and Actuators B: Chemical* 174 (2012): 87-93.

[14] Ke, Ming-Tsun, et al. "A MEMS-based benzene gas sensor with a self-heating WO3 sensing layer." *Sensors* 9.4 (2009): 2895-2906.

[15] Patel, S. V., et al. "Chemicapacitive microsensors for volatile organic compound detection." *Sensors and Actuators B: Chemical* 96.3 (2003): 541-553.

[16] Park, Kwan Kyu. "Capacitive Micromachined Ultrasonic Transducer (CMUT) for Chemical Detection in Air. " *Diss. Stanford University* (2011).

[17] Fine, George F., et al. "Metal oxide semi-conductor gas sensors in environmental monitoring." *Sensors* 10.6 (2010): 5469-5502.

[18] O'sullivan, C. K., and G. G. Guilbault. "Commercial quartz crystal microbalances–theory and applications." *Biosensors and bioelectronics* 14.8 (1999): 663-670.

[19] Fanget, S., et al. "Gas sensors based on gravimetric detection—A review." *Sensors and Actuators B: Chemical* 160.1 (2011): 804-821.

[20] Jakubik, Wiesław P. "Surface acoustic wave-based gas sensors." *Thin Solid Films* 520.3 (2011): 986-993.

[21] Kuhl, W., G. R. Schodder, and F-K. Schröder. "Condenser transmitters and microphones with solid dielectric for airborne ultrasonics." *Acta Acustica united with Acustica* 4.5 (1954): 519-532.

[22] Ergun, Arif S., Goksen G. Yaralioglu, and Butrus T. Khuri-Yakub. "Capacitive micromachined ultrasonic transducers: Theory and technology." *Journal of Aerospace Engineering* 16.2 (2003): 76-84.

[23] Haller, Matthew I., and Butrus T. Khuri-Yakub. "A surface micromachined electrostatic ultrasonic air transducer." *IEEE Transactions on Ultrasonics, Ferroelectrics, and Frequency Control* 43.1 (1996): 1-6.

[24] Chen, Albert I. "Row-Column Capacitive Micromachined Ultrasonic Transducers for Medical Imaging." *University of Waterloo* (2016).

[25] Haller, Matthew I., and Butrus T. Khuri-Yakub. "A surface micromachined electrostatic ultrasonic air transducer." *IEEE Transactions on Ultrasonics, Ferroelectrics, and Frequency Control* 43.1 (1996): 1-6.

[26] Wong, Lawrence. "Capacitive Micromachined Ultrasonic Transducers for Non-destructive Testing Applications." *University of Waterloo* (2014).

[27] Niklaus, Frank, and J. Q. Lu. "Handbook of Wafer Bonding." (2012).

[28] Tsuji, Yukihide, Mario Kupnik, and Butrus T. Khuri-Yakub. "Low temperature process for CMUT fabrication with wafer bonding technique." *Ultrasonics Symposium (IUS), 2010 IEEE*. IEEE, 2010.

[29] Bengtsson, Stefan, and Petra Amirfeiz. "Room temperature wafer bonding of silicon, oxidized silicon, and crystalline quartz." *Journal of Electronic Materials* 29.7 (2000): 909-915.

[30] Wong, Serena H., et al. "Capacitive micromachined ultrasonic transducers for therapeutic ultrasound applications." *IEEE transactions on Biomedical Engineering* 57.1 (2010): 114-123.

[31] Jagannathan, Hemanth, et al. "Micro-fluidic channels with integrated ultrasonic transducers." *Ultrasonics Symposium, 2001 IEEE*. Vol. 2. IEEE, 2001.

[32] Li, Zhenhao. "Fabrication of Capacitive Micromachined Ultrasonic Transducers based on Adhesive Wafer Bonding." *University of Waterloo* (2017).

[33] Oralkan, Omer, et al. "Experimental characterization of collapse-mode CMUT operation." *ieee transactions on ultrasonics, ferroelectrics, and frequency control* 53.8 (2006): 1513-1523.

[34] Logan, Andrew, and John TW Yeow. "Fabricating capacitive micromachined ultrasonic transducers with a novel silicon-nitride-based wafer bonding process." *IEEE transactions on ultrasonics, ferroelectrics, and frequency control* 56.5 (2009).

[35] Erguri, A. S., et al. "Capacitive micromachined ultrasonic transducers: fabrication technology." *IEEE transactions on ultrasonics, ferroelectrics, and frequency control* 52.12 (2005): 2242-2258.

[36] Huang, Yongli, et al. "Fabricating capacitive micromachined ultrasonic transducers with wafer-bonding technology." *Journal of microelectromechanical systems* 12.2 (2003): 128-137.

[37] Andrew Stephan Logan. “The Design, Fabrication and Characterization of Capacitive Micromachined Ultrasonic Transducers for Imaging Applications.” *University of Waterloo* (2010).

[38] Muralt, Paul, et al. "Piezoelectric actuation of PZT thin-film diaphragms at static and resonant conditions." *Sensors and Actuators A: Physical* 53.1 (1996): 398-404.

[39] Wong, Lawrence LP, et al. "A feasibility study of piezoelectric micromachined ultrasonic transducers fabrication using a multi-user MEMS process." *Sensors and Actuators A: Physical* 247 (2016): 430-439.

[40] Baborowski, Jacek, et al. "Simulation and characterization of piezoelectric micromachined ultrasonic transducers (pMUTs) based on PZT/SOI membranes." *International Journal of Computational Engineering Science* 4.03 (2003): 471-475.

[41] Akasheh, Firas, et al. "Development of piezoelectric micromachined ultrasonic transducers." *Sensors and Actuators A: Physical* 111.2 (2004): 275-287.

[42] Akasheh, Firas, et al. "Piezoelectric micromachined ultrasonic transducers: Modeling the influence of structural parameters on device performance." *IEEE transactions on ultrasonics, ferroelectrics, and frequency control* 52.3 (2005): 455-468.

[43] Lu, Yipeng, Amir Heidari, and David A. Horsley. "A high fill-factor annular array of high frequency piezoelectric micromachined ultrasonic transducers." *Journal of Microelectromechanical Systems* 24.4 (2015): 904-913.

[44] Qiu, Yongqiang, et al. "Piezoelectric micromachined ultrasound transducer (PMUT) arrays for integrated sensing, actuation and imaging." *Sensors* 15.4 (2015): 8020-8041.

[45] Yamashita, Kaoru, et al. "Arrayed ultrasonic microsensors with high directivity for in-air use using PZT thin film on silicon diaphragms." *Sensors and Actuators A: Physical* 97 (2002): 302-307.

[46] Jung, Joontaek, et al. "Fabrication of a two-dimensional piezoelectric micromachined ultrasonic transducer array using a top-crossover-to-bottom structure and metal bridge connections." *Journal of Micromechanics and Microengineering* 23.12 (2013): 125037.

[47] Sammoura, Firas, Katherine Smyth, and Sang-Gook Kim. "Optimizing the electrode size of circular bimorph plates with different boundary conditions for maximum deflection of piezoelectric micromachined ultrasonic transducers." *Ultrasonics* 53.2 (2013): 328-334.

[48] Colinet, Eric, et al. "Self-oscillation conditions of a resonant nanoelectromechanical mass sensor." *Journal of Applied Physics* 105.12 (2009): 124908.

[49] Fanget, S., et al. "Gas sensors based on gravimetric detection—A review." *Sensors and Actuators B: Chemical* 160.1 (2011): 804-821.

[50] Bachman, Mark. "RCA-1 silicon wafer cleaning." *INRF application note Engineering of Microworld at the University of California. Irvine* (1999).

[51] Leissa, Arthur W. *Vibration of plates*. OHIO STATE UNIV COLUMBUS (1969).

[52] De, Sudipto K., and N. R. Aluru. "Full-Lagrangian schemes for dynamic analysis of electrostatic MEMS." *Journal of Microelectromechanical Systems* 13.5 (2004): 737-758.

[53] Liu, Xiao, et al. "A survey on gas sensing technology." *Sensors* 12.7 (2012): 9635-9665.

[54] Bhuyan, Anshuman, et al. "Integrated circuits for volumetric ultrasound imaging with 2-D CMUT arrays." *IEEE transactions on biomedical circuits and systems* 7.6 (2013): 796-804.

[55] Qiu, Yongqiang, et al. "Piezoelectric micromachined ultrasound transducer (PMUT) arrays for integrated sensing, actuation and imaging." *Sensors* 15.4 (2015): 8020-8041.

[56] Wygant, Ira O., Mario Kupnik, and Butrus T. Khuri-Yakub. "Analytically calculating membrane displacement and the equivalent circuit model of a circular CMUT cell." *Ultrasonics Symposium, 2008. IUS 2008. IEEE*. IEEE, 2008.

[57] Lu, Yipeng, et al. "Broadband piezoelectric micromachined ultrasonic transducers based on dual resonance modes." *Micro Electro Mechanical Systems (MEMS), 2015 28th IEEE International Conference on*. IEEE, 2015.

[58] Lu, Yipeng, Stefon Shelton, and David A. Horsley. "High frequency and high fill factor piezoelectric micromachined ultrasonic transducers based on cavity SOI wafers." *Proc. Solid-State Sensors, Actuators and Microsystems Workshop*. 2014.

[59] Wang, Tao, Takeshi Kobayashi, and Chengkuo Lee. "Micromachined piezoelectric ultrasonic transducer with ultra-wide frequency bandwidth." *Applied Physics Letters* 106.1 (2015): 013501.

# Appendix A

Code 1:

```
clc;
clear all;
a=(250E-6); %half length
b=(250E-6); %half width
h=10E-6;
E=156E+9;
u=0.215;
rho=2.33E+3;
h2=0.5E-6;
E2=300E+9;
u2=0.22;
rho2=3.3E+3;
%%
D=E*h^3/(12*(1-u^2));
w=9/(a*a)*sqrt(D/(h*rho)) % single plate: rad/s
f=w/(2*pi)    % single plate: Hz
%%
B1=E2/(1-u2^2)*h2+E/(1-u^2)*h;
C1=1/2*E2/(1-u2^2)*((h+h2)^2-h^2)+1/2*E/(1-u^2)*(h^2);
D1=1/3*E2/(1-u2^2)*((h+h2)^3-h^3)+1/3*E/(1-u^2)*(h^3);
Dc=(B1*D1-C1^2)/B1
w2=9/a^2*sqrt(Dc/(h*rho+h2*rho2)) % laminated plate: rad/s
f2=w2/(2*pi)    %laminated plate: Hz
```

Code 2:

```
clc;
clear all;
a=(110E-6); %half length
b=(110E-6); %half width
```

```
h=10E-6;
E=156E+9;
u=0.215;
rho=2.33E+3;
h2=0.5E-6;
E2=300E+9;
u2=0.22;
rho2=3.3E+3;
%%
D=E*h^3/(12*(1-u^2));
w=9/(a*a)*sqrt(D/(h*rho)) % single plate: rad/s
f=w/(2*pi)    % single plate: Hz
%%
B1=E2/(1-u2^2)*h2+E/(1-u^2)*h;
C1=1/2*E2/(1-u2^2)*((h+h2)^2-h^2)+1/2*E/(1-u^2)*(h^2);
D1=1/3*E2/(1-u2^2)*((h+h2)^3-h^3)+1/3*E/(1-u^2)*(h^3);
Dc=(B1*D1-C1^2)/B1
w2=9/a^2*sqrt(Dc/(h*rho+h2*rho2)) % laminated plate: rad/s
f2=w2/(2*pi)    %laminated plate: Hz
```

Code 3:

```
clc;clear
a = 25e-6; %cell radius in m
tm = 605e-9; %thickness of membrane in m
v = 0.27; %poisson's ratio SiN
E = 290e9; %young's modulus in Pa SiN
rho = 3000; %density of membrane material SiN kg/m3
e_m = 7.5; %relative permitivity of SiN
rhom = 890; %%%%%%%%%density of veg oil
e0= 8.85e-12; %%%%%%%%%permitivity of vacuum
di_strength = 5.3e6; %dielectric strength of photo BCB V/cm
e_ins = 2.65; %relative permitivity of photo BCB
```

```
t_gap = 378e-9; %gap height m
t_ins= 1059e-9; %insulation layer m
geff=t_gap + t_ins/e_ins + tm/e_m; %effecitve gap
w0_num = (2.95*tm)/(a^2) * sqrt(E/(rho*(1-v^2)));
w0_denom = sqrt(1+0.67*rhom*a/(rho*tm));
f0_air = w0_num/(2*pi);
f0_oil = (w0_num/w0_denom)/(2*pi);
X=['Resonant Frequency in air is ', num2str(f0_air/1e6,3),'MHz'];
disp(X)
X=['Resonant Frequency in oil is ', num2str(f0_oil/1e6,3),'MHz'];
disp(X)
c=1440; %speed of sound in m/s
half_lamda = c/f0_oil*1e6/2;
X=['Max Pitch is ', num2str(half_lamda),'um'];
disp(X)
w0 = 2*pi*f0_air;
A = pi*a^2;
meq = A*tm;
k=w0^2*1.86*rho*meq;
Vpi = sqrt((8*k*geff^3)/(27*A*e0));
X=['pull in voltage is ', num2str(Vpi,3),'V'];
disp(X)
V_break = di_strength*100*t_ins;
X=['Breakdown Voltage is ', num2str(V_break),'V'];
disp(X)
```

Code 4：

```
clc;
clear all;
a=(23E-6); %half length
h=605E-9;
E=290E+9;
```

```
u=0.27;
rho=3000;
h2=1311E-9;
E2=2.9E+9;
u2=0.34;
rho2=957;
%%
B1=E2/(1-u2^2)*h2+E/(1-u^2)*h;
C1=1/2*E2/(1-u2^2)*((h+h2)^2-h^2)+1/2*E/(1-u^2)*(h^2);
D1=1/3*E2/(1-u2^2)*((h+h2)^3-h^3)+1/3*E/(1-u^2)*(h^3);
Dc=(B1*D1-C1^2)/B1;
w2=10.21/a^2*sqrt(Dc/(h*rho+h2*rho2)); % laminated plate: rad/s
f2=w2/(2*pi)    %laminated plate: Hz
```